

# Effect of hyaluronic acid hydrogels containing astrocyte-derived extracellular matrix and/or V2a interneurons on histologic outcomes following spinal cord injury



Russell E. Thompson<sup>a, b</sup>, Jennifer Pardieck<sup>a, b</sup>, Laura Smith<sup>c</sup>, Peter Kenny<sup>a</sup>, Lindsay Crawford<sup>b</sup>, Molly Shoichet<sup>c</sup>, Shelly Sakiyama-Elbert<sup>a, \*</sup>

<sup>a</sup> Department of Biomedical Engineering, University of Texas at Austin, 107 W Dean Keeton, Austin, TX 78712, USA

<sup>b</sup> Department of Biomedical Engineering, Washington University in St Louis, 1 Brookings Drive, St Louis, MO 63130, USA

<sup>c</sup> Department of Chemical Engineering & Applied Chemistry, University of Toronto, 200 College Street, Toronto, ON M5S 3E5, Canada

## ARTICLE INFO

### Article history:

Received 13 November 2017

Received in revised form

9 January 2018

Accepted 4 February 2018

Available online 6 February 2018

### Keywords:

Mouse embryonic stem cells

Tissue engineering

Neural engineering

## ABSTRACT

One reason for the lack of regeneration, and poor clinical outcomes, following central nervous system (CNS) injury is the formation of a glial scar that inhibits new axon growth. In addition to forming the glial scar, astrocytes have been shown to be important for spontaneous SCI recovery in rodents, suggesting some astrocyte populations are pro-regenerative, while others are inhibitory following injury. In this work, the effect of implanting hyaluronic acid (HA) hydrogels containing extracellular matrix (ECM) harvested from mouse embryonic stem cell (mESC)-derived astrocytes on histologic outcomes following SCI in rats was explored. In addition, the ability of HA hydrogels with and without ECM to support the transplantation of mESC-derived V2a interneurons was tested. The incorporation of ECM harvested from protoplasmic (grey matter) astrocytes, but not ECM harvested from fibrous (white matter) astrocytes, into hydrogels was found to reduce the size of the glial scar, increase axon penetration into the lesion, and reduce macrophage/microglia staining two weeks after implantation. HA hydrogels were also found to support transplantation of V2a interneurons and the presence of these cells caused an increase in neuronal processes both within the lesion and in the 500  $\mu\text{m}$  surrounding the lesion. Overall, protoplasmic mESC-derived astrocyte ECM showed potential to treat CNS injury. In addition, ECM:HA hydrogels represent a novel scaffold with beneficial effects on histologic outcomes after SCI both with and without cells.

© 2018 Elsevier Ltd. All rights reserved.

## 1. Introduction

One of the major inhibitors of spinal cord regeneration is the glial scar that develops around the spinal cord lesion [1]. This scar has a stereotyped morphology with astrocytes forming a scar penumbra that represents both a physical barrier, due the woven morphology of astrocyte processes, and a biochemical barrier to new axon growth. One major class of axon growth inhibitors present within the glial scar is chondroitin sulfate proteoglycans (CSPGs) [2]. Degradation of CSPGs with the enzyme chondroitinase ABC has been shown to improve SCI outcomes in rodents, indicating the importance of CSPGs in axon growth inhibition [3,4]. These

observations, coupled with the role astrocytes play in the formation of a physical barrier in the glial scar, led to the belief that astrocytes are primarily inhibitory following SCI.

Recent studies have challenged the conclusion that astrocytes are solely inhibitory following SCI, with astrocyte knockout studies demonstrating that astrocytes are required for recovery following SCI. In particular, glial fibrillary acid protein (GFAP)-thymidine kinase (TK) mice, which allow ganciclovir administration to be used to ablate all dividing GFAP<sup>+</sup> cells, have been used to study the conditional ablation of astrocytes either at the time of injury or 5 weeks post injury. These studies have found that the lack of astrocytes around the SCI lesion acutely results in a larger lesion area and decreased axonal growth into the lesion [5,6]. Delivery of ganciclovir 5 weeks after injury caused delayed scar ablation, but it did not result in increased axonal growth suggesting that the presence of astrocytes is required for axon growth even in the

\* Corresponding author.

E-mail address: [sakiyama@utexas.edu](mailto:sakiyama@utexas.edu) (S. Sakiyama-Elbert).

absence of the scar at later time points. Furthermore, it was found that hydrogel-based delivery of neurotrophin-3 (NT-3) and brain-derived neurotrophic factor (BDNF) improved axon penetration into the lesion only when the glial scar was intact [6]. These data suggest that some astrocytes can promote axon growth following SCI, and that they are required for recovery.

These knockout observations are supported by recent astrocyte reactivity studies, which found that reactive astrocytes exist on a phenotypic spectrum from pro-regenerative to inhibitory for axon growth [7]. One illustration of this reactivity spectrum is the changes in astrocyte phenotype depending on insult. In particular, an inflammatory insult from lipopolysaccharide has been found to lead to inhibitory reactive astrocytes, while an ischemic insult leads to pro-regenerative reactive astrocytes [8]. In addition, cytokines have also been found to manipulate reactive astrocyte phenotype as well, with acute IL-6 exposure promoting inhibitory, scar astrocytes [9,10] and IL-10 promoting pro-regenerative astrocytes [11]. These observations suggest that there is a role of the immune response in regulating the regenerative potential of astrocytes.

Astrocyte populations from different regions of the central nervous system (CNS) have also been found to have different responses to injury. Injury to fibrous (white matter) astrocytes has been found to cause process hypertrophy and overlap reminiscent of the glial scar [12], while protoplasmic (grey matter) astrocytes exhibit minimal process overlap following injury [13]. Functional differences between protoplasmic and fibrous astrocyte populations have also been observed in transplantation following right-side cervical dorsal column transection SCI. In particular, transplantation of human or mouse glial restricted progenitor-derived astrocytes exhibiting a protoplasmic phenotype led to improved outcomes, both histologically and behaviorally, compared to transplantation of astrocytes exhibiting a fibrous phenotype [14,15]. Recently, methods were developed to specifically derive these astrocyte populations from mouse embryonic stem cells (mESCs). Studies of *in vitro* neuron growth on substrates derived from these astrocytes revealed that neurons extended significantly longer neurites on protoplasmic-derived substrates than fibrous-derived substrates, particularly when only decellularized extracellular matrix (ECM) from each type of astrocyte was tested [16].

The ability of astrocyte-derived ECM alone to support neurite extension is particularly appealing because ECMs often contain many bioactive molecules that can promote regeneration [17]. The capacity for ECM to promote regeneration has been harnessed to improve recovery from bone and cartilage injury [18], peripheral nerve injury [19] and myocardial infarction [20]. Importantly for implantation into patients, ECM xenografts have been successfully used without any indication of immune rejection from the host [21–23]. Given both their bioactivity and low immunogenicity, compared to cell transplantation, ECM-based materials have significant appeal for promoting tissue regeneration; however, many ECM-derived materials require animal sacrifice for tissue harvest. One way to avoid the animal harvest requirement is to derive ECMs from *in vitro* cell sources, such as ESC-derived or induced pluripotent stem cells (iPSCs)-derived cell populations. One drawback to *in vitro* harvested ECM is that they do not form a hydrogel without additional crosslinking. This means that the *in vitro* ECM needs to be incorporated into a gelation system or crosslinked to be useable as a scaffold.

Hyaluronic acid (HA) plays the major structural role in the native CNS ECM and naturally binds to other CNS ECM components, such as fibronectin, CSPGs and heparin sulfate proteoglycans [24], making HA a logical choice as a base scaffold for SCI treatment [25]. HA is degraded by hyaluronidase and thus needs to be crosslinked to be stable after implantation. The Diels–Alder click-reaction

between HA-furan and polyethylene glycol (PEG)-bismaleimide results in an injectable, biocompatible HA hydrogel that forms under physiological conditions [26,27]. Injectability of the hydrogel is a desirable trait since it allows the entire, irregular lesion cavity to be filled without requiring significant dissection of the glial scar to create space [28].

Interneurons are the main neuronal population that facilitates local connectivity between spinal cord neurons. This role makes interneurons key for coordination, left-right alteration, reflex circuits, and central pattern generation. Interestingly, rodents have been found to demonstrate recovery from spatially and temporally separated left and right lateral transections, but not just spatially separated left and right lateral transections. This suggests that local rewiring, which is likely due to local interneuron populations, is important for spontaneous recovery from SCI [29]. One interneuron population that has known involvement in spontaneous SCI recovery is V2a interneurons. These cells have been implicated as required for normal left-right alternation in the lumbar spinal cord, especially at high speeds of locomotion, as well as respiratory recovery following cervical SCI [30–32]. Recently, a mESC line has been developed that allows for highly enriched populations of V2a interneurons to be derived *in vitro*, making transplantation of this specific interneuron population possible [33,34].

This work examines the effect of HA hydrogels containing ECM derived from different mESC-derived astrocyte populations on motoneuron growth *in vitro* and the effects of these astrocyte ECMs on histologic outcomes in rats following a thoracic dorsal hemisection SCI. The ability of HA hydrogels with and without ECM to support transplantation of mESC-derived V2a interneurons into a SCI lesion is also explored. This work represents the first implantation of an astrocyte-derived ECM for the treatment of SCI. The utility of the implanted ECM was found to depend on the phenotype of the astrocyte-containing population from which it was produced. Fibrous ECM (F-ECM) was found to confer no benefit and in some cases detrimental histological outcomes, while protoplasmic ECM (P-ECM) was found to decrease the size of the glial scar, decrease macrophage/microglia infiltration, and increase axonal ingrowth. mESC-derived V2a interneurons were found to survive in HA hydrogels both with and without incorporation of protoplasmic ECM, and the presence of V2a interneurons was found to increase the presence of neuronal processes within and around the SCI lesion. These data demonstrate a novel material platform that shows significant promise as a material for development of future CNS injury treatments.

## 2. Materials and methods

### 2.1. mESC culture

RW4 (ATCC, SCRC-1018), Hb9-PAC CAG-TdTomato and Chx10-PAC bact-TdTomato mESCs were maintained in complete media (CM) (10% Fetal Bovine Serum (Invitrogen, Carlsbad, CA), 10% Newborn Calf Serum (Invitrogen), 132  $\mu$ M beta mercaptoethanol (BME) (Sigma, St Louis, MO), 10,000 units/mL mouse leukemia inhibitory factor (Life Technologies, Carlsbad, CA) and passaged every 2–3 days (60–80% confluency). 0.25% Trypsin-EDTA (Life Technologies) incubation at 37 °C for 5 min was used to dissociate mESCs from the culture flask. This reaction was then quenched with fresh CM and cells were seeded into a new T25 flask coated with 0.1% gelatin (Sigma).

### 2.2. Astrocyte ECM production

Fibrous and protoplasmic populations were derived from RW4 ESCs as previously described (Fig. 1A) [16]. Briefly,  $1 \times 10^6$  RW4

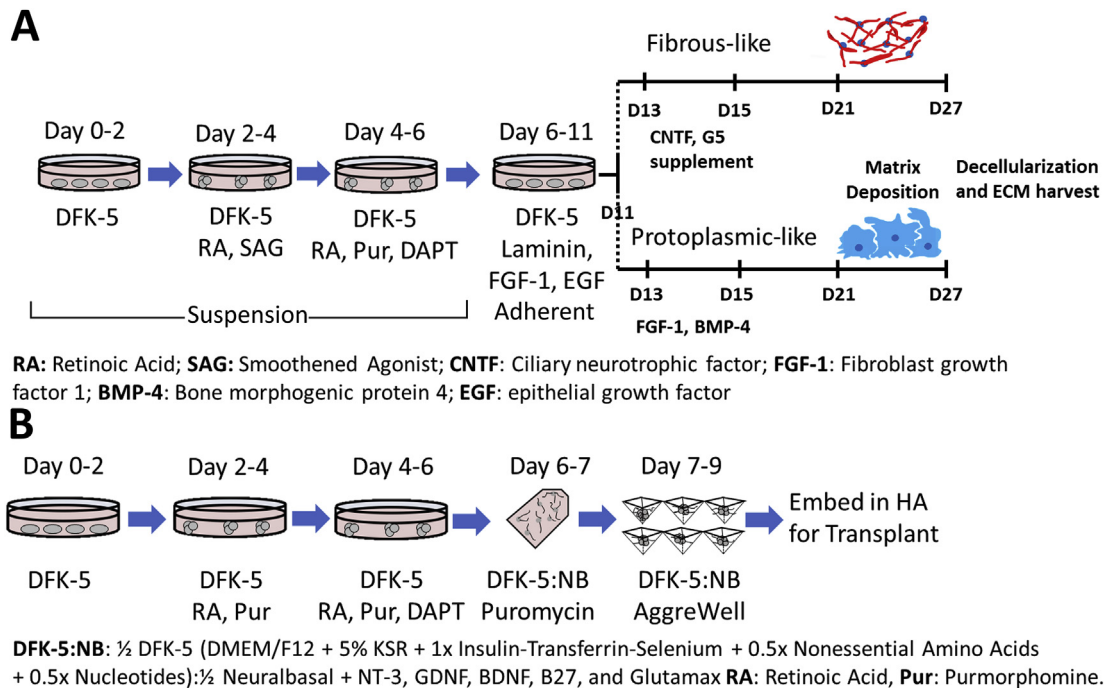


**Fig. 1. Schematic representation of astrocyte ECM production and V2a derivation.** A) Protoplasmic-like and fibrous-like astrocytes were derived from mouse embryonic stem cells (mESCs) using a 15-day protocol. Following the 15 days of induction, astrocytes were allowed to mature in appropriate media for 6 days (D15–D21) prior to being seeded for matrix deposition (D21–27). After deposition, plates were decellularized, and the ECM scraped off the plates and lyophilized in 50 mM trehalose solution. B) V2a interneurons were derived from a mESC line that expresses puromycin resistance under the control of the Chx10 promoter and has constitutively active TdTomato expression. Following selection, interneurons were seeded onto aggregewell plates for 2 days to allow neuroaggregates to form prior to embedding them into HA hydrogels.

ESCs were cultured in suspension on agar-coated 10 cm dishes in 10 mL DFK5 (DMEM/F12 (Life Technologies) plus 5% Knockout Serum Replacement (Life Technologies), 50  $\mu$ M nonessential amino acids (Life Technologies), 1x Insulin-Transferrin-Selenium (Life Technologies), 100  $\mu$ M beta-mercaptoethanol (Sigma), 5  $\mu$ M thymidine, and 15  $\mu$ M of the following nucleosides: adenosine, cytosine, guanosine, and uridine (Life Technologies) for two days to form embryoid bodies (EBs) followed by 4 days in 10 mL DFK5 plus 2  $\mu$ M RA and 600 nM Smoothened Agonist (SAG) [35]. On day 6, EBs were dissociated and  $4 \times 10^6$  cells were seeded onto a gelatin-coated low adherence 10 cm dish (ThermoFisher) in DFK5 media plus 20 ng/mL epithelial growth factor (EGF) (Peprotech, Rocky Hill, NJ), 10 ng/mL fibroblast growth factor 1 (FGF-1) (Peprotech) and 1  $\mu$ g/mL laminin (Fisher Scientific) for 5 days. On day 11, the cultures were switched into lineage-specific media for 10 additional days. Fibrous media: DMEM/F12 plus 1x G5 supplement (Invitrogen), 10  $\mu$ g/mL ciliary neurotrophic factor (CNTF) (Peprotech); Protoplasmic media: DFK5 plus 10  $\mu$ g/mL FGF-1, 10  $\mu$ g/mL bone morphogenetic protein 4 (BMP4) (Peprotech).

At D21, astrocytes were seeded onto gelatin-coated TC treated 10 cm dishes (ThermoFisher) at a density of 20,000 cells/cm<sup>2</sup> and culture in appropriate lineage media for 6 days to allow for matrix deposition. After matrix deposition, cells were removed from the culture plates using a modified Hudson decellularization protocol [36]. Following decellularization, 1 mL of 50 mM trehalose was added to each plate and the proteins on the plate were scraped from the plate surface with a cell scraper. The resulting suspension of ECM proteins was then lyophilized overnight and stored at  $-20^\circ\text{C}$  until use in hydrogels.

### 2.3. Preparation of V2a interneuron neuroaggregates

V2a interneurons were generated from Chx10-PAC bact-

TdTomato mESCs as previously described [33]. After induction, EBs were dissociated with 0.25% trypsin and  $2.5 \times 10^7$  cells were seeded onto a poly-L-ornithine/laminin coated T25 flask. Chx10<sup>+</sup> cells were then selected in half neural basal (Life Technologies)-half DFK5 media with 1x GlutaMAX (Life Tech), 1x B27, 2  $\mu$ g/mL puromycin and 10 ng/mL of the following growth factors for 24 h: glial-derived neurotrophic factor (GDNF) (Peprotech), NT-3 (Peprotech), and BDNF (Peprotech). After selection, neurons were lifted from the flasks using Accutase<sup>®</sup> (Sigma) treatment for 30 min and then 500,000 cells/well were placed into an AggreWell 400 plate with 1200 small aggregation wells (Stemcell Technologies, Vancouver, BC). V2a interneurons were maintained in V2a neuronal media (half neurobasal-half DFK5 media plus 1x GlutaMAX, 1x B27, and 10 ng/mL of the following growth factors: BDNF, GDNF, NT-3) on the AggreWell<sup>™</sup> plate for 2 days to allow for neuroaggregate formation (Fig. 1B) [37]. After aggregate formation, neuroaggregates were washed from the AggreWell plates with 100  $\mu$ L of V2a neuronal media.

### 2.4. Preparation of HA hydrogels

30% conjugated HA-furan and 39% conjugated HA-methylfuran were synthesized as previously described from 250 MDa MW HA (Creative PEGWorks, Chapel Hill, NC) [26,61]. Percent conjugation signifies the percentage of carboxylic acid groups within the HA macromolecules that have been reacted to add the furan functional group. For ECM incorporation, lyophilized ECMs were dissolved in 50  $\mu$ L water and the protein concentration determined using a Pierce 660 nm assay (ThermoFisher) according to manufacturer instructions. All hydrogels had a final HA concentration of 1 mg/mL and a 3.5:3.0 M ratio of the PEG-bismaleimide (Creative PEGWorks) crosslinking molecule to furan groups added. For *in vitro* motoneuron assays, ECM was added to 2 mg/mL HA-furan at different

weight ratios prior to PEG addition, and then sterile phosphate-buffered saline, pH 7.4 (PBS) was added until final HA concentration was 1 mg/mL. To form thin HA gels, 50  $\mu$ L of gel was added to each well of a 48 well plate, and the plates were incubated overnight at 37 °C prior to motoneuron seeding.

For acellular implantation studies: 2 mg/mL HA-furan was dissolved in water, or 50 mM trehalose for HA alone implantation, followed by addition of the reconstituted astrocyte ECM at a 1:100 wt ratio of ECM to HA, and finally the solution was diluted with sterile PBS. PEG-bismaleimide was then added and 50  $\mu$ L of gel solution was loaded into a Hamilton syringe and the syringe placed at 37 °C overnight to allow gelation to occur prior to implantation. For V2a interneuron transplantation: HA-methylfuran was dissolved in V2a neuronal media at a concentration of 4 mg/mL, and then astrocyte ECM was added at a 1:100 wt ratio of ECM to HA followed by addition of sufficient neuroaggregate suspension to obtain a final concentration of approximately 6 NAs/ $\mu$ L. The final solution was then diluted with V2a neuronal media to 1 mg/mL HA. The neuroaggregate number used results in roughly 60 NAs, or 25,000 cells, being transplanted per animal. Once the gel solution was prepared, 50  $\mu$ L of gel was loaded into a Hamilton syringe, and the syringe placed at 37 C for 2 h to allow gelation to occur prior to transplantation.

### 2.5. Motoneuron culture on thin HA hydrogels

Motoneurons were derived from Hb9-Puro CAG-TdTomato mESCs that constitutively express TdTomato under the control of the synthetic CAG promoter, as previously described [38]. To obtain pure motoneuron cultures, EBs were selected with 4  $\mu$ g/mL puromycin from day 5–6 prior to dissociation and seeding onto the prepared HA hydrogels at a density of 20,000 cells/cm<sup>2</sup>. Motoneurons were then cultured in half DFK5 and half Neurobasal media plus 1x B27 and imaged daily over the next 2 days. To facilitate automated analysis, a single motoneuron was imaged per 20x field to ensure the entire neuron was included with the image. A minimum of 3 neurons were imaged per well with 3 wells used per condition for each of the 4 replicates performed.

### 2.6. Dorsal hemisection surgery

All animal procedures used in this work were approved by the Institutional Animal Care and Use Committee at the University of Texas at Austin, followed the NIH Guide for the Care and Use of Laboratory Animals, and were supported by the Animal Resources Center at the University of Texas at Austin. Animals (female Long-Evans rats, 225–275 g, Envigo, Indianapolis, IN) were anesthetized with 1.5–5% isoflurane and subcutaneous (SQ) injection of 5 mg/kg xylazine, surgery was performed on a heated pad. A single incision was made through the skin on the back from

approximately T4 to T12, then blunt dissection was used to expose the muscular layer. Parallel cuts were made on either side of the spinal cord from T7 to T10 and the muscles along the spinal cord were retracted. To expose the spinal cord, a T8 dorsal laminectomy was performed using fine tipped rongeurs and the dura mater was removed with fine-tipped tweezers and microscissors.

To ensure a consistent injury, the spinal column was stabilized with spinal clamps attached to a stereotactic frame (Narishige, Tokyo, JP) and vitrectomy scissors, attached a micromanipulator, were lowered 1.5 mm into the spinal cord. To ensure a consistent dorsal hemisection, three cuts were administered at three separate locations moving from left to right across the entire spinal cord. Following hemisection, the muscular layer was closed with degradable suture and the skin stapled closed. Post-op animals were given cefazolin (25 mg/kg SQ) to limit infection and cefazolin injections were continued 2x/day for 5 days. For pain management, animals were given buprenorphine (0.04 mg/kg SQ) 2x/day for the first 2 days post-op followed by 0.01 mg/kg SQ buprenorphine injections 2x/day for an additional 3 days. Bladders were expressed manually 2x/day until spontaneous bladder emptying resumed.

### 2.7. Hydrogel transplantation surgery

Two weeks after the dorsal hemisection procedure was performed, injured spinal cords were re-exposed via the same approach used in the injury surgery. Once the spinal cord was exposed, a small hole was made in the scar tissue to allow access into the SCI lesion cavity for a blunt-tipped Hamilton syringe. HA hydrogels were prepared as described above and 10  $\mu$ L of gel was injected into each lesion cavity, which is sufficient gel to slightly overfill the cavities. For sham implants, the lesion cavity was exposed as in the HA implantation animals and 10  $\mu$ L sterile 50 mM trehalose was injected. For the acellular implantation study animals were divided into 4 groups: sham implant, HA alone, HA + Fibrous ECM (F-ECM), HA + Protoplasmic ECM (P-ECM) (Table 1). In the V2a interneuron transplantation study animals were divided into 5 groups: sham implant, HA-mF alone, HA + P-ECM, HA + Cells (V2a interneuron neuroaggregates), HA + P-ECM + Cells (V2a interneuron neuroaggregates) (Table 2). Post-op care was performed as in the injury surgeries, all animals in the V2a interneuron transplantation study were immune suppressed with daily SQ injections of cyclosporine-A (10 mg/kg, Novartis, Basel, CH) starting on the day of transplantation and continuing for the duration of the study.

Two weeks after the transplantation surgery animals were euthanized via overdose of FatalPlus (pentobarbital) and transcardial perfusion was performed with 4% paraformaldehyde (PFA) (Fisher Scientific) in phosphate buffered saline (PBS). After dissection, spinal cords were post-fixed in 4% PFA for 4 h at 4 °C and washed overnight with phosphate buffer at 4 °C prior to being cryoprotected in 30% sucrose in water for 3 days at 4 °C.

**Table 1**

Study design of acellular implantation study to compare astrocyte ECM effects on SCI recovery.



Treatment Group	N
Sham Implant (Injury Only)	8
HA alone Implant	8
HA + Fibrous Astrocyte ECM (F-ECM)	7
HA + Protoplasmic Astrocyte ECM (P-ECM)	8

**Table 2**

Study design of V2a interneuron transplantation study to confirm benefits of P-ECM incorporation in a different HA hydrogel and explore the ability of HA hydrogels to support cell transplantation.



Treatment Group	N
Sham Implant (Injury Only)	7
HA alone Implant	7
HA + Protoplasmic Astrocyte ECM (P-ECM)	7
HA + V2a Interneuron Aggregates (Cells)	8
HA + P-ECM + Cells	8

Cryoprotected cords were embedded in Tissue-Tek OCT compound, frozen and cut into 20  $\mu\text{m}$  sagittal sections on a Leica CM1950 cryostat.

### 2.8. Immunohistochemistry

After sectioning, immunohistochemistry (IHC) was performed on 7 spinal cord sections, spaced 200  $\mu\text{m}$  apart, for each animal in the study. For cord staining, OCT was washed from the slides with PBS and the sections were permeabilized with 0.1% Triton X-100 for 15 min. Following permeabilization, cord sections were washed 3x with PBS and blocked with 5% normal goat serum in PBS (NGS) for 1 h. Primary antibodies were then applied overnight at 4 °C at the following dilutions in 2% NGS: Tuj-1 (BioLegend, San Diego, CA, Clone AA-10, 1:1000), GFAP (ImmunoStar, Hudson, WI, 1:100), chondroitin sulfate (CS56, Sigma, 1:250), CD68 (ED1, Bio-Rad Antibodies, Oxford, UK, 1:200), CD8 $\alpha$  (Bio-Rad Antibodies, 1:1000), CD11b (Bio-Rad Antibodies, 1:1000), NeuN (EMD Millipore, Billerica, MA, 1:500), VGlut-2 (Millipore, 1:1000), NeuN (Millipore, 1:500). Following primary incubation, cords were washed 3x with PBS and were then incubated for 2 h at room temperature in a 1:500 dilution of the appropriate AlexaFluor secondary antibody (Life Technologies) in 2% NGS. Finally, cords were washed 3 times with PBS and the sections mounted using ProLong Gold anti-fade reagent with DAPI (Life Technologies).

### 2.9. Immunohistochemistry image analysis

To quantify IHC staining, tile scan images were taken using a CMOS camera attached to a Leica DMI8 inverted fluorescent microscope with a 10 $\times$  objective. Lesion areas were then traced using ImageJ and the traced lesion expanded by 500  $\mu\text{m}$  to assess the host response to the implant. The resulting lesion area and lesion area +500  $\mu\text{m}$  images were quantified using a custom Matlab (Mathworks, Natick, MA) script as previously described [4]. This script determines the intensity of each pixel and then determines whether the pixel is positive or negative for a given stain based on a user defined threshold. To facilitate comparison between animals and groups, all sections for a given group were stained, imaged, and analyzed at the same time. Additionally, data reported represents percent positive area for each stain which is defined as (positive pixels/all non-black pixels)\*100. Using this approach helps to control for sectioning artifacts that result holes in the section. Quantification for the 500  $\mu\text{m}$  surrounding the lesion alone was achieved by subtracting the positive and total pixel count in the lesion only image from the equivalent pixel counts in the lesion +500  $\mu\text{m}$  images. For colocalization analysis, images were processed using CellProfiler (Broad Institute, Cambridge, MA) and

the number of pixels positive for both the stain of interest (Tuj-1 or VGlut-2) and TdTomato was quantified.

### 2.10. Statistics

*In vitro* data was analyzed by two-way ANOVA with a Bonferroni post-hoc correction using a 95% confidence threshold. For *in vivo* studies, significance was determined using the non-parametric Kruskal-Wallis analysis of variance followed by Dunn's test to determine significance with 95% confidence. Power analysis was performed prior to starting the *in vivo* studies. Both studies were powered to show a 30% difference with 80% confidence.

## 3. Results

### 3.1. Protoplasmic ECM incorporation improves motoneuron growth on HA hydrogels

Previous work has demonstrated that motoneurons exhibited longer neurite extension on decellularized mESC-derived protoplasmic astrocyte substrates than decellularized mESC-derived fibrous astrocyte substrates [16]. Since decellularization leaves only the ECM on the plate [36], the ability of ECMs harvested from decellularized mESC-derived astrocyte substrates to improve motoneuron growth was explored. To form a growth substrate, ECM was combined with a previously described HA-furan PEG-bismaleimide hydrogel system. This HA system was chosen because of the gentle crosslinking reaction and its ability to be used *in vivo*. To preserve bioactivity, ECM was scraped from decellularized plates into 50 mM trehalose and then lyophilized. The resulting ECM powder was then dissolved in water with HA-furan in three different weight to weight ratios of ECM to HA (1:500, 1:100, 1:25 ECM:HA) prior to the addition of the PEG-bismaleimide crosslinker. A thin layer of gel was then allowed to form overnight in the culture plate prior to motoneuron seeding.

Motoneuron growth on ECM:HA hydrogels was assessed after 48 h, and it was found that 1:25 Fibrous ECM (F-ECM) to HA, and 1:100 and 1:25 Protoplasmic ECM (P-ECM) to HA gels significantly improved motoneuron neurite extension when compared to HA gels with no added ECM (Fig. 2B, C, F, H). There was also a trend demonstrating some dose dependency of the ECM with increasing ECM concentration improving neurite growth as evidenced by 1:100 P-ECM:HA (20,464  $\pm$  2415 (Std. Err) pixels/nucleus) showing significantly improved growth compared to 1:500 P-ECM:HA (11,956  $\pm$  2022 (Std. Err) pixels/nucleus) (Fig. 2E). Finally, P-ECM demonstrated greater potency than F-ECM as illustrated by motoneurons extending significantly longer neurites on 1:100 P-ECM:HA (20,464  $\pm$  2415 (Std. Err) pixels/nucleus) gels than 1:100 F-

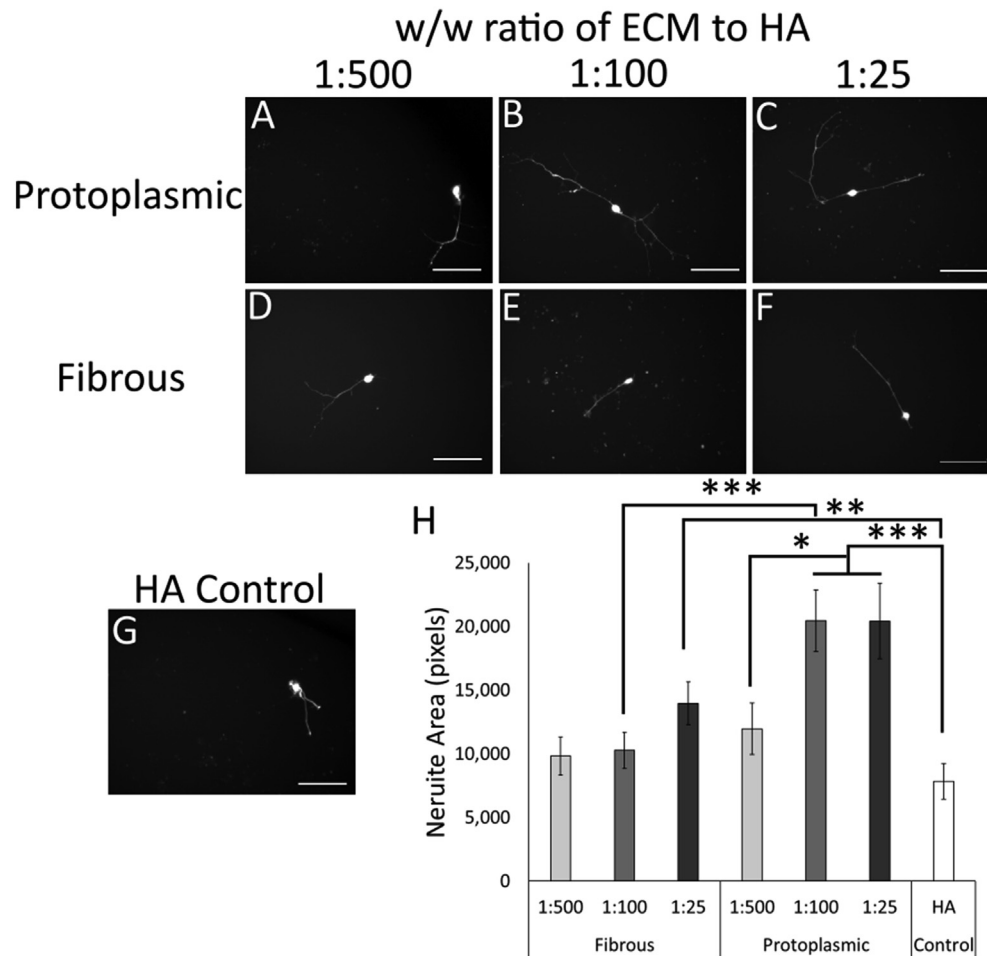


**Fig. 2. Protoplasmic ECM incorporation improves motoneuron growth after 48 h in culture on HA hydrogels.** Ratios given are weight of ECM to weight of HA. Specifically, 1:500 gels have 100 ng ECM and 50  $\mu$ g HA; 1:100 gels have 500 ng ECM and 50  $\mu$ g HA; and, 1:25 gels have 2  $\mu$ g ECM and 50  $\mu$ g HA. **A–C)** Representative images of motoneurons grown on different HA hydrogel substrate after 48 h. **A–C)** HA hydrogels containing protoplasmic ECM; **D–E)** HA hydrogels containing fibrous ECM. Scale bars: 100  $\mu$ m. **H)** Quantification of neurite area/nucleus of motoneurons after 48 h in culture. Error bars = std error, n = 25–45, \*: p < 0.05, \*\*: p < 0.01, \*\*\*: p < 0.001.

ECM:HA gels ( $10,276 \pm 1423$  (Std. Err) pixels/nucleus) (Fig. 2B, E, H). These data indicate that ECM can be harvested from mESC-derived astrocyte cultures, and that the ECM maintains its ability to support neuronal growth. Based on these *in vitro* results, 1:100 ECM:HA ratio gels were used to determine the effect of astrocyte-derived ECM on histologic outcomes following SCI *in vivo*.

### 3.2. Protoplasmic ECM can be detected in HA hydrogels *in vitro* and *in vivo*

Next, the ability of the HA hydrogels to retain ECM *in vivo* and *in vitro* was investigated using antibodies against collagen XII $\alpha$ 1. Collagen XII $\alpha$ 1 staining was used because previous proteomic data showed that collagen XII $\alpha$ 1 was the most prevalent protein within P-ECM that was significantly enriched in P-ECM over F-ECM, and it is too large to readily diffuse away [16]. Immunohistochemistry revealed that the collagen XII $\alpha$ 1 within the P-ECM could be detected in P-ECM:HA gels, but not in HA alone gels after 1 week *in vitro*, and that the incorporated collagen XII $\alpha$ 1 forms aggregates that are over 100  $\mu$ m across within the gel (Figure S1A, B). Beyond 1 week *in vitro* the gels began to lose integrity.

Collagen XII $\alpha$ 1 staining was also used to determine if the P-ECM was present two weeks after implantation into a SCI lesion. Staining revealed collagen XII $\alpha$ 1 aggregates within the SCI lesion of animals

implanted with P-ECM:HA gels that were similar in size to those observed in the *in vitro* staining (Figure S1B, D). These aggregates were not present in animals transplanted with HA alone gels, but more diffuse collagen XII $\alpha$ 1 staining was detected in the HA alone and P-ECM:HA gels suggesting that some native cells within the SCI lesion produce collagen XII $\alpha$ 1 (Figure S1C).

With collagen XII $\alpha$ 1 staining indicating the continued presence of implanted ECM for up to 2 weeks *in vivo*, the effect of F-ECM and P-ECM on histological outcomes after SCI was explored to determine whether the observed *in vitro* effects of astrocyte ECMs translated into any *in vivo* effects. To address this question, a sub-acute implantation model in rats was used where a T8 dorsal hemisection SCI was performed, followed two weeks later by an implantation (treatment) surgery. The two-week delay between injury and treatment allows the glial scar and lesion cavity to fully develop and stabilize in size. This limits the continued expansion of the lesion following implantation, which can impede the ability of native cells to penetrate the implant [39]. Rats were chosen for this work because rats, like humans, tend to cavitate following SCI. Furthermore, the use of a mouse ECM in rats could demonstrate the therapeutic viability of xenogenic ECM. Two weeks after implantation, histological changes resulting from HA gel implantation were assessed by immunohistochemistry staining for immune cells, astrocytes, and neurons.

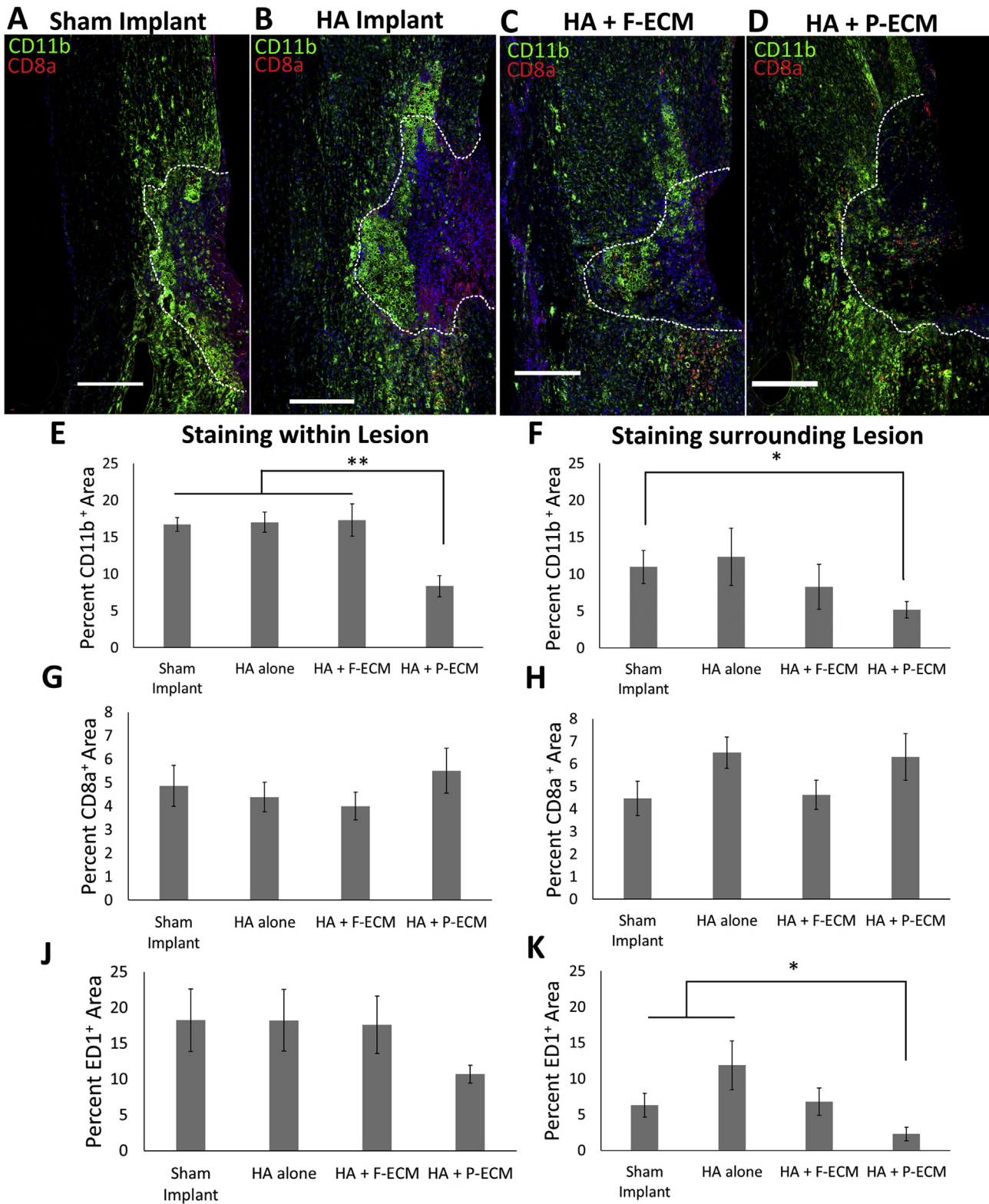


**Fig. 3. Protoplasmic ECM decreases immune cell infiltration into a SCI lesion.** **A-D** Representative images of CD8a (Cytotoxic T-cells, red) staining and the CD11b (myeloid lineage cells, green) staining 2 weeks after implantation (4 weeks after injury). Scale bars: 500  $\mu$ m, dashed line denotes lesion boundary. **E,F** Quantification of CD11b<sup>+</sup> area both within the SCI lesion (**E**) and in the 500  $\mu$ m surrounding the SCI lesion (**F**). **G,H** Quantification of CD8a<sup>+</sup> area both within the SCI lesion (**G**) and in the 500  $\mu$ m surrounding the SCI lesion (**H**). **J,K** Quantification of ED1<sup>+</sup> area (macrophages) both within the SCI lesion (**J**) and in the 500  $\mu$ m surrounding the SCI lesion (**K**). \*:  $p < 0.05$ , \*\*:  $p < 0.01$ .  $n = 7$  HA + Fibro ECM, 8 for all other groups. (For interpretation of the references to colour in this figure legend, the reader is referred to the Web version of this article.)

### 3.3. Protoplasmic ECM modulates host immune response in acellular implants

Since the ECMs used for this study were harvested from mouse cells and transplanted into a rat host, it was important to ensure that there were no signs of implant rejection by the immunocompetent host. The immune response to HA hydrogel implantation was assessed with staining for CD11b (general myeloid cell marker), CD8a (cytotoxic T-cell marker), and ED-1 (CD68) (marker of activated macrophages and microglia). Immune staining revealed no signs of rejection of the xenogenic ECM based on the lack of any increase in immune cell staining in the presence of ECM (Fig. 3). In fact, the implantation of P-ECM:HA gels was found to significantly reduce infiltration of myeloid cells (CD11b<sup>+</sup> area) into the lesion compared to all other groups (P-ECM:  $8.3 \pm 1.4$  (Std. Err.)% vs Sham:  $17 \pm 0.93$  (Std. Err.)%) (Fig. 3A–E), and decrease CD11b staining around the lesion compared to the sham implant group (P-ECM:  $5.2 \pm 1.1$  (Std. Err.)% vs Sham:  $11 \pm 2.2$  (Std. Err.)%) (Fig. 3A, D, F). Staining for microglia and macrophages (ED-1<sup>+</sup> area) was found to mirror the pattern observed in the CD11b staining with P-ECM incorporation causing a significant decrease in the percent ED-1<sup>+</sup> area surrounding the lesion compared to both the sham implant group and the HA hydrogel group (P-ECM:  $5.5 \pm 0.97$  (Std. Err.)% vs Sham:  $9.7 \pm 1.6$  (Std. Err.)%) (Fig. 3J–K).

### 3.4. Protoplasmic ECM incorporation decreases the presence of inhibitory CSPGs and size of the glial scar following acellular implantation

The glial scar forms around the lesion core following SCI and is known to represent both a physical and biochemical barrier to axonal regeneration following SCI. To determine the level of astrocyte reactivity, GFAP (a pan-reactive astrocyte marker) was used. The production of inhibitory molecules within the cords was also determined with an antibody against CS56, which detects CSPGs. GFAP staining revealed that P-ECM:HA gel implantation decreased the size of the glial scar (based on percent GFAP<sup>+</sup> area in the 500  $\mu$ m surrounding the lesion) compared to both the sham implant group and the F-ECM:HA implant group (P-ECM:  $9.7 \pm 1.1$  (Std. Err.)% vs Sham:  $16 \pm 3.3$  (Std. Err.)%) (Fig. 4A, C–D, F). CS56 staining also showed that P-ECM:HA gels decreased the presence of inhibitory CSPGs within the lesion (Fig. 4A, D, G). The presence of the HA itself was sufficient to cause a decrease in the presence of inhibitory CSPGs in the glial scar (500  $\mu$ m surrounding the lesion); interestingly, this effect was lost in the F-ECM:HA gel group, but maintained in the P-ECM:HA gel group (P-ECM:  $9.8 \pm 1.6$  (Std. Err.)% vs Sham:  $15 \pm 1.8$  (Std. Err.)%) (Fig. 4A–D, H). Taken together these data show that the type of astrocyte ECM within the implant affects the response of the host astrocytes to the HA hydrogels with P-ECM decreasing the GFAP<sup>+</sup> area surrounding the lesion and F-ECM potentially negating the reduction in CSPG staining surrounding the lesion seen in the HA alone group.

### 3.5. Protoplasmic ECM incorporation increases neurite growth into a SCI lesion following acellular implantation

With encouraging results in terms of the immune and astrocyte reaction to P-ECM:HA gels, the next important question was whether these scaffolds had any impact on the growth of axons into the SCI lesion. This is important to measure since the penetration of native axons into the transplanted material could aid in future reconnection of the signaling pathways within the spinal cord. Staining for  $\beta$ -tubulin III (Tuj-1) was used to assess the presence of neuronal processes within and around the SCI lesions. Based on percentage of the lesion/border area staining positive for  $\beta$ -tubulin

III, it was found that P-ECM:HA gels increased axonal growth into the lesion compared to both the sham implant control and the F-ECM:HA gel group (P-ECM:  $14 \pm 1.0$  (Std. Err.)% vs Sham:  $9.2 \pm 1.9$ , F-ECM  $8.0 \pm 0.6$  (Std. Err.)%) (Fig. 5A–E). This increase in  $\beta$ -tubulin III indicates that the presence of P-ECM improves the ability of native neurons to extend into the SCI lesion and glial scar environment, consistent with the improvement seen in *in vitro* neuron growth in the presence of P-ECM (Fig. 2) [16].

Overall, P-ECM:HA hydrogel implantation appeared to improve histological outcomes following SCI injury, so the ability of these hydrogels to support the transplantation of a neuronal population was explored. For cellular transplantation within the HA gels to be possible, the HA crosslinking had to be modified to accelerate the gelation kinetics to enable viable cell encapsulation. Changing from HA-furan to HA-methylfuran (HA-mF) was recently described as a method that utilizes the same crosslinking chemistry and material properties, but allows for faster gelation [40]. By maintaining as much of the same material properties and similar chemistry, it seemed likely that the P-ECM:HA-mF gel implants would exhibit the same benefits that were observed in P-ECM:HA implants.

### 3.6. Protoplasmic ECM maintains immunomodulatory effects in the presence of systemic immune suppression

Recently there has been increased interest in the ability of interneurons to support local rewiring and hence facilitate spontaneous recovery following SCI. Thus far interneuron transplantation has largely focused on inhibitory, GABAergic interneuron precursors that are isolated from the forebrain. These interneurons have been successfully transplanted into the spinal cord, and they have been shown to integrate and improve post-SCI pain and bladder function [41,42]. Recently, a Chx10-PAC mESC line has been developed that allows for derivation of highly enriched V2a interneurons [33]. Since V2a interneurons have been suggested as an important type of neuron for local rewiring and represent an excitatory population, mESC-derived V2a interneurons with constitutively active TdTomato were used in this study. To facilitate survival thru transplantation, V2a interneurons were aggregated with approximately 420 cells/neuroaggregate using an AggreWell™ plate before addition to the HA solution prior to gelation. Roughly 60 neuroaggregates were transplanted into each animal resulting in a total of ~25,000 cells per transplant. This cell transplantation study had 5 groups: sham implant (to allow for comparison to the acellular study), HA-mF alone, HA-mF + P-ECM, HA-mF + Cells and HA-mF + P-ECM + Cells (Table 2).

To confirm that immune suppression was sufficient and to compare to the macrophage/microglia findings of the acellular study, ED-1 staining was performed on sections from the second *in vivo* study. Quantification of ED-1 staining revealed that, similar to what was observed in the acellular implantation study, P-ECM significantly decreased the percentage of the lesion area stained positive for ED1 compared to sham and HA-mF alone (P-ECM:  $11 \pm 3.2$  (Std. Err.)% vs Sham:  $19 \pm 2.8$  (Std. Err.)%) (Figure S2F). The percent ED1<sup>+</sup> area was also found to be significantly lower in the 500  $\mu$ m surrounding the lesion in P-ECM transplantation than the sham implant group (P-ECM:  $3.6 \pm 0.9$  (Std. Err.)% vs Sham:  $6.1 \pm 1.1$  (Std. Err.)%) (Figure S2F–G). Importantly there was no indication of a significant increase in ED-1 staining when the neuroaggregates were transplanted, indicating sufficient immune suppression (Figure S2A, D–E, F–G).

### 3.7. Incorporation of V2a interneurons decreases GFAP staining while HA-mF decreases inhibitory CSPG staining

Staining for GFAP and CS56 in the cellular transplantation study

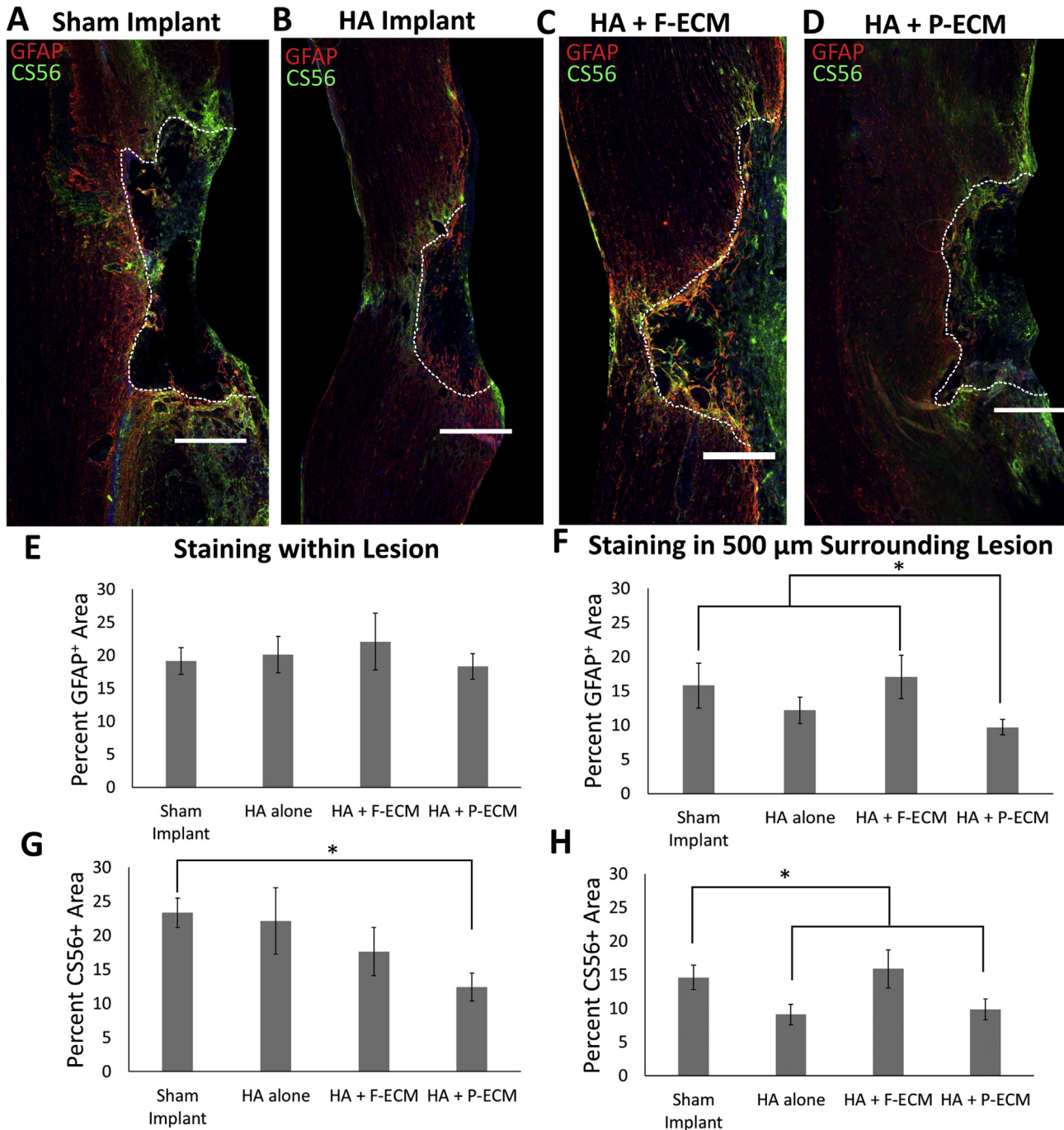


**Fig. 4.** HA reduces CSPG staining and protoplasmic ECM incorporation decreases GFAP area. **A–D)** Representative images of CS56 (inhibitory CSPGs, green) staining and the GFAP (reactive astrocytes, red) staining 2 weeks after implantation (4 weeks after injury). Scale bars: 500 μm, dashed line denotes lesion boundary. **E,F)** Quantification of GFAP<sup>+</sup> area both within the SCI lesion (E) and in the 500 μm surrounding the SCI lesion (F). **G,H)** Quantification of CS56<sup>+</sup> area both within the SCI lesion (G) and in the 500 μm surrounding the SCI lesion (H). \*:  $p < 0.05$ , \*\*:  $p < 0.01$ .  $n = 7$  HA + Fibro ECM, 8 for all other groups. (For interpretation of the references to colour in this figure legend, the reader is referred to the Web version of this article.)

revealed similar effects on the glial scar to those observed in the acellular implantation study. In particular, the presence of HA-mF hydrogels seemed to be sufficient to significantly decrease inhibitory CSPG staining within the 500 μm surrounding the lesion (HA-mF:  $3.8 \pm 0.9$  (Std. Err.)% vs Sham:  $15 \pm 3.4$  (Std. Err.)%) (Fig. 6A–C, G). Similar to the acellular study, the percent GFAP<sup>+</sup> area was found to be significantly decreased in the presence of P-ECM compared to both sham and HA alone groups (P-ECM:  $8 \pm 1.9$  (Std. Err.)% vs Sham:  $15 \pm 2.6$  (Std. Err.)%) (Fig. 6J, S3). The GFAP staining was also

found to be altered in the presence of the V2a neuroaggregates with both cellular groups showing significantly less GFAP staining within and around the lesion than the HA alone group (HA-mF surrounding lesion:  $18 \pm 1.9$  (Std. Err.)% vs HA-mF + Cells surrounding lesion:  $11 \pm 1.1$  (Std. Err.)%) (Fig. 6B, D–E, H–J). These observations indicate that HA-mF has the same effect on the scar astrocytes as observed in the HA-furan and that P-ECM incorporation causes GFAP downregulation regardless of the HA used.

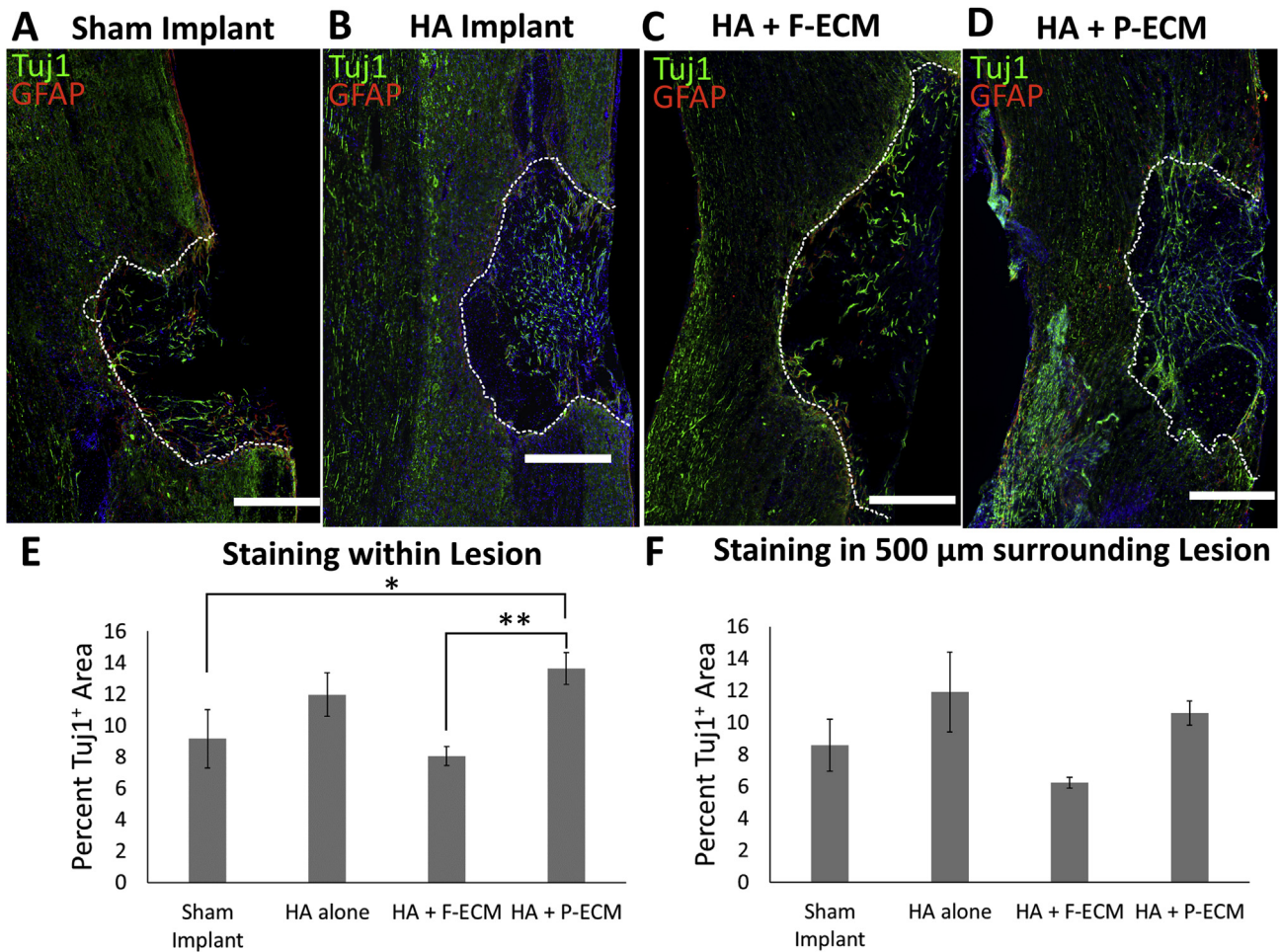


**Fig. 5. Protoplasmic ECM incorporation increases neural fiber staining within an SCI lesion.** A–D) Representative images of  $\beta$ -tubulin III (neurons, green) staining and the GFAP (reactive astrocytes, red) staining 2 weeks after implantation (4 weeks after injury). Scale bars: 500  $\mu$ m, dashed line denotes lesion boundary. E, F) Quantification of Tuj1<sup>+</sup> area both within the SCI lesion (E) and in the 500  $\mu$ m surrounding the SCI lesion (F). \*:  $p < 0.05$ , \*\*:  $p < 0.01$ .  $n = 7$  HA + Fibro ECM, 8 for all other groups. (For interpretation of the references to colour in this figure legend, the reader is referred to the Web version of this article.)

### 3.8. V2a interneuron aggregates survive within HA-mF hydrogels and P-ECM:HA hydrogels and increase neuronal process staining within and surrounding the SCI lesion

Since there was no sign of immune rejection of transplants, the presence of V2a Interneurons within the lesion was assessed by quantifying TdTomato fluorescence. The percentage of the area within the SCI lesion found to be TdTomato<sup>+</sup> was significantly higher in the HA + Cells and the HA + P-ECM + Cells group than the associated acellular hydrogel groups (P-ECM + Cells:  $6.4 \pm 1.3$  (Std. Err.)% vs P-ECM:  $3.7 \pm 0.36$  (Std. Err.)%) (Fig. 7B–F). However, this difference did not extend to the 500  $\mu$ m surrounding the lesion (Fig. 7G). It is important to note that there is autofluorescence at 555 nm so there is some apparent “TdTomato positive” area in the animals that had no transplanted cells. Together these observations suggest that the V2a neuroaggregates are surviving with the gel for up to 2 weeks following transplantation.

Based on the continued presence of V2a neuroaggregates within the SCI lesion, staining for  $\beta$ -tubulin III was performed to see if the presence of V2a neuroaggregates resulted in an increase of area staining positive for neuronal processes within and around the lesion.  $\beta$ -tubulin III staining revealed a similar pattern among the acellular groups as observed in the first *in vivo* study with HA + P-ECM demonstrating significantly more neural fibers than either HA

or sham within the SCI lesion (P-ECM:  $15 \pm 1.5$  (Std. Err.)% vs Sham:  $8.8 \pm 2.0$  (Std. Err.)%) (Fig. 7H). The presence of cells also resulted in a significant increase of  $\beta$ -tubulin III within the lesion compared to both the sham implant and the HA alone implant groups (Fig. 7H).  $\beta$ -tubulin III staining surrounding the lesion was also found to be significantly increased in HA + P-ECM, HA + Cells, and HA + P-ECM + Cells when compared to HA alone (HA-mF:  $9.6 \pm 2.1$  (Std. Err.)% vs HA-mF + Cells:  $17 \pm 1.7$  (Std. Err.)%) (Fig. 7J). Furthermore, animals with HA + P-ECM + Cells transplants were found to have a significantly higher percentage of  $\beta$ -tubulin III<sup>+</sup> area around the lesion than sham transplant animals (P-ECM + Cells:  $15 \pm 2.6$  (Std. Err.)% vs Sham:  $7.9 \pm 2.7$  (Std. Err.)%) (Fig. 7J).

### 3.9. Transplanted cells maintain V2a identity, extend neural processes within and around lesion, and migrate into host spinal cord

To determine whether transplanted V2a interneurons maintained a glutamatergic, neuronal identity, colocalization between TdTomato fluorescence and staining for  $\beta$ -tubulin III, vesicular glutamate transporter 2 (VGlut-2), or neuronal nuclei (NeuN) was assessed. Visual inspection of cord sections revealed locations both within and around the lesion where these stains colocalized with TdTomato (Fig. 8A–C). The presence this colocalization around the

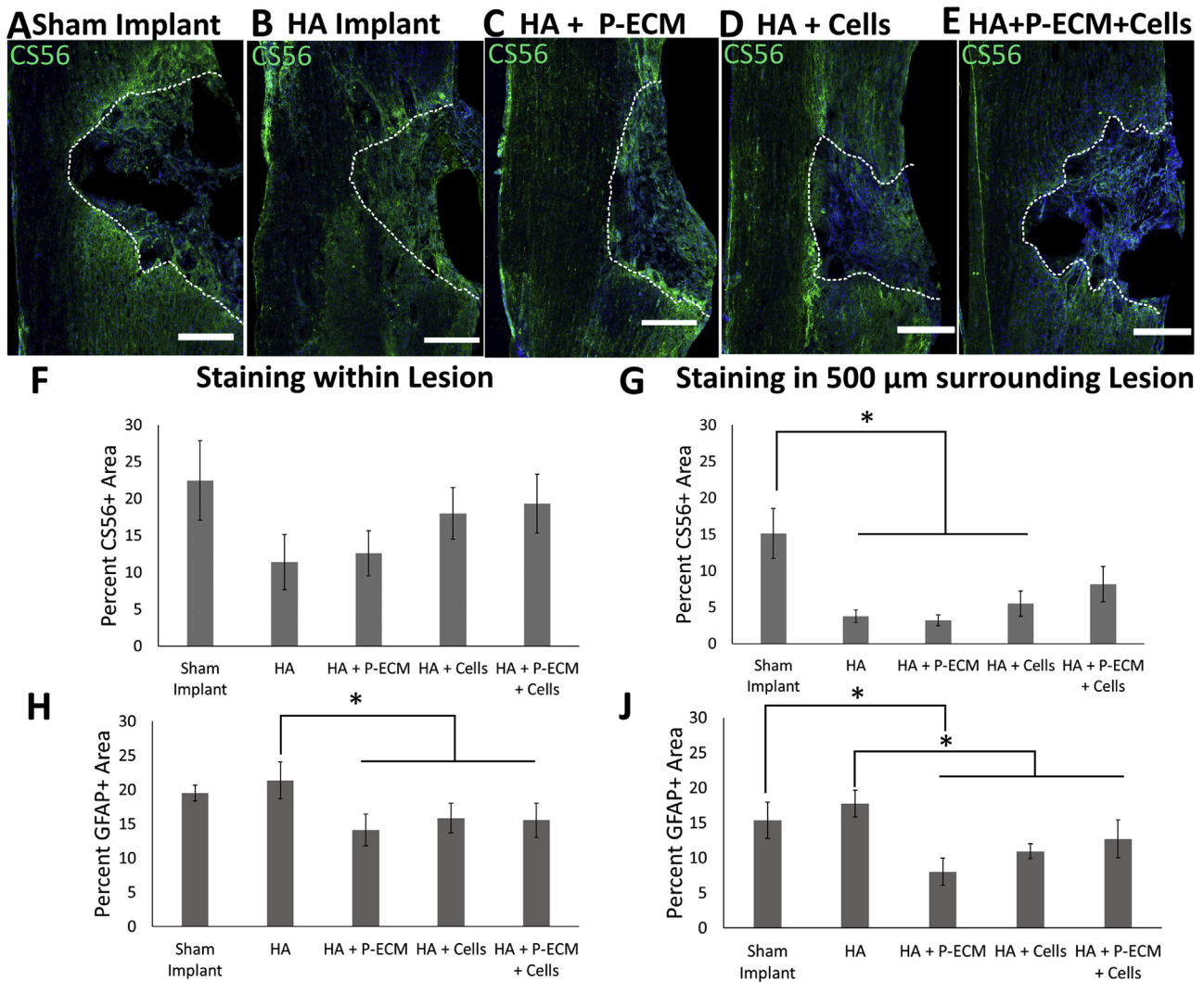


**Fig. 6. Hydrogel implantation modulates the response of the host astrocytes. A–E** Representative images of CS56 staining (inhibitory CSPGs, green) 2 weeks after implantation (4 weeks after injury). Scale bars: 500  $\mu\text{m}$ , dashed line denotes lesion boundary. **F,G** Quantification of CS56<sup>+</sup> area both within the SCI lesion (F) and in the 500  $\mu\text{m}$  surrounding the SCI lesion (G). **H,J** Quantification of GFAP<sup>+</sup> area both within the SCI lesion (H) and in the 500  $\mu\text{m}$  surrounding the SCI lesion (J). \*:  $p < 0.05$ .  $n = 7$  for Sham, HA, and HA + Proto ECM, 8 for HA + Cells and HA + Proto ECM + Cells. (For interpretation of the references to colour in this figure legend, the reader is referred to the Web version of this article.)

lesion suggests that the transplanted interneurons could migrate into the host spinal cord. The percent of area within and around the lesion that was positive for both  $\beta$ -tubulin III and TdTomato was quantified to determine the level of neuronal process extension from the transplanted cells both within the lesion and in the host. This analysis found that the cellular groups exhibited significantly more colocalization than the acellular groups, indicating that the transplanted V2a NAs extended neuronal processes (P-ECM within lesion:  $0.32 \pm 0.14$  (Std. Err.)% vs P-ECM + Cells within lesion:  $1.2 \pm 0.56$  (Std. Err.)% (Fig. 8D–E).

Similar quantification was performed on VGlut-2 staining and it was found that the HA + P-ECM + Cells group had significantly more colocalization of VGlut-2<sup>+</sup> and TdTomato<sup>+</sup> both within the lesion and in the 500  $\mu\text{m}$  surrounding the lesion than any of the acellular groups (P-ECM within lesion:  $0.39 \pm 0.085$  (Std. Err.)% vs P-ECM + Cells within lesion:  $0.83 \pm 0.14$  (Std. Err.)% (Fig. 8F–G). Together these observations suggest that the V2a neuroaggregates are surviving within the HA hydrogels and that they continue to be glutamatergic. These data also suggest that some combination of the neuroaggregates extending neuronal processes and the host

increasing axonal growth (perhaps due to the presence of the neuroaggregates) accounts for the observed increase in  $\beta$ -tubulin III<sup>+</sup> area both within and around the SCI lesion in the HA + Cells group compared to the HA alone group.

#### 4. Discussion

##### 4.1. HA hydrogel implantation decreases inhibitory CSPG staining within the glial scar and protoplasmic astrocyte ECM incorporation decreases astrocyte reactivity

Assessment of inhibitory CSPGs using CS56 staining revealed that the presence of either HA-furan or HA-mF hydrogels within the lesion area resulted in decreased staining for CSPGs in the 500  $\mu\text{m}$  surrounding the lesion (Figs. 4 and 6). Downregulation of CSPGs staining has been previously described in response to acute implantation of either a photo-crosslinked high molecular weight HA hydrogel or a poly-L-lysine (PLL) modified HA hydrogel [43,44]. This effect has been found to be dependent on the molecular weight of the HA with lower molecular HA (40–400 kDa) observed

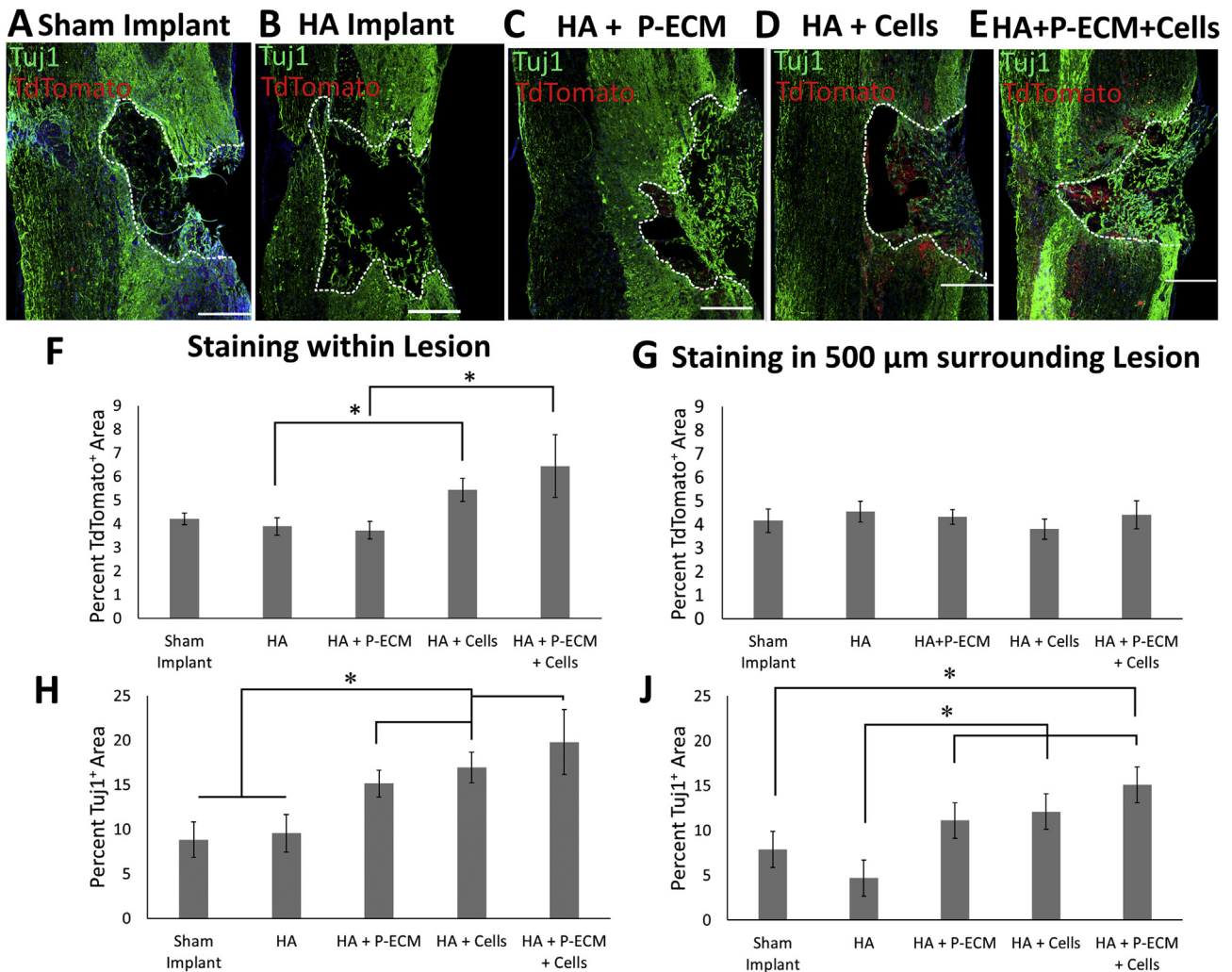


**Fig. 7. Protoplasmic ECM and transplanted V2a interneurons increase neuronal staining following spinal cord injury.** A–E) Representative images of  $\beta$ -tubulin III staining (neurons, green) and tdTomato (transplanted cells, red) 2 weeks after implantation (4 weeks after injury). Scale bars: 500  $\mu$ m. F,G) Quantification of the percent TdTomato<sup>+</sup> area both within the SCI lesion (F) and in the 500  $\mu$ m surrounding the SCI lesion (G). H,J) Quantification of percent Tuj1<sup>+</sup> area both within the SCI lesion (H) and in the 500  $\mu$ m surrounding the SCI lesion (J). (For interpretation of the references to colour in this figure legend, the reader is referred to the Web version of this article.)

to cause an upregulation of CSPG expression and an increase in the size of glial scar [45]. In the present studies, HA hydrogel implantation is found to cause a similar downregulation of CSPG expression when delivered two weeks after injury, unlike the acute treatment used in previous studies. This effect of HA on CSPG expression has not been observed in implantation studies of fibrin [4], fetal spinal cord ECM [46], or methylcellulose hydrogels [47] following SCI. This suggests that the observed decrease in CSPG expression might be a specific benefit of HA hydrogels.

Despite the decrease in CSPG area, there was no observed downregulation of GFAP in the presence of HA hydrogels compared the sham implant animals (Figs. 4 and 6). GFAP immunoreactivity in response to material implantation has been found to be highly variable across with some materials, such as fibrin, leading to decreased GFAP<sup>+</sup> area [48,49], while others, such as poly(lactic-co-glycolic acid) (PLGA) and gelatin sponges, increased GFAP immunoreactivity [50]. Incorporation of P-ECM was found to reduce the percent GFAP<sup>+</sup> area in the 500  $\mu$ m surrounding the lesion with both HA hydrogel formulations tested compared to sham implantation. The HA + P-ECM hydrogels were also found to demonstrate a similar decrease in CSPG staining as observed in the HA alone hydrogels (Figs. 4 and 6). This finding suggests that P-ECM presence

may help to reduce the reactivity and/or hypertrophy of native astrocytes surrounding the lesion, while maintaining the benefits of HA on CSPG expression.

Interestingly, the beneficial effects of HA implantation on the glial scar was largely lost when a F-ECM:HA hydrogel was implanted. This change is evidenced by the significant increase in GFAP staining in the 500  $\mu$ m surrounding the lesion in F-ECM:HA implanted animals compared to P-ECM:HA implanted groups, and the loss of the HA-associated CSPG reduction in the F-ECM:HA group (Fig. 4). This suggests that F-ECM incorporation may result in some phenotype switch of native astrocytes toward a more inhibitory phenotype, which results in the observed increase in astrocyte reactivity and CSPG production. The concept of ECM components affecting astrocyte phenotype is not new, with astrocytes known to upregulate a “scar” phenotype in response to the integrin binding to certain ECM components, such as collagen I [51,52]. Studies of some of the major proteins found to be upregulated in P-ECM compared to F-ECM, namely fibronectin and aggrecan [16], have also been found to decrease GFAP and CSPG expression by astrocytes *in vitro* [53]. These studies provide a potential basis for further experiments to identify the specific components within F-ECM and P-ECM that cause these apparent changes in native astrocyte phenotype.

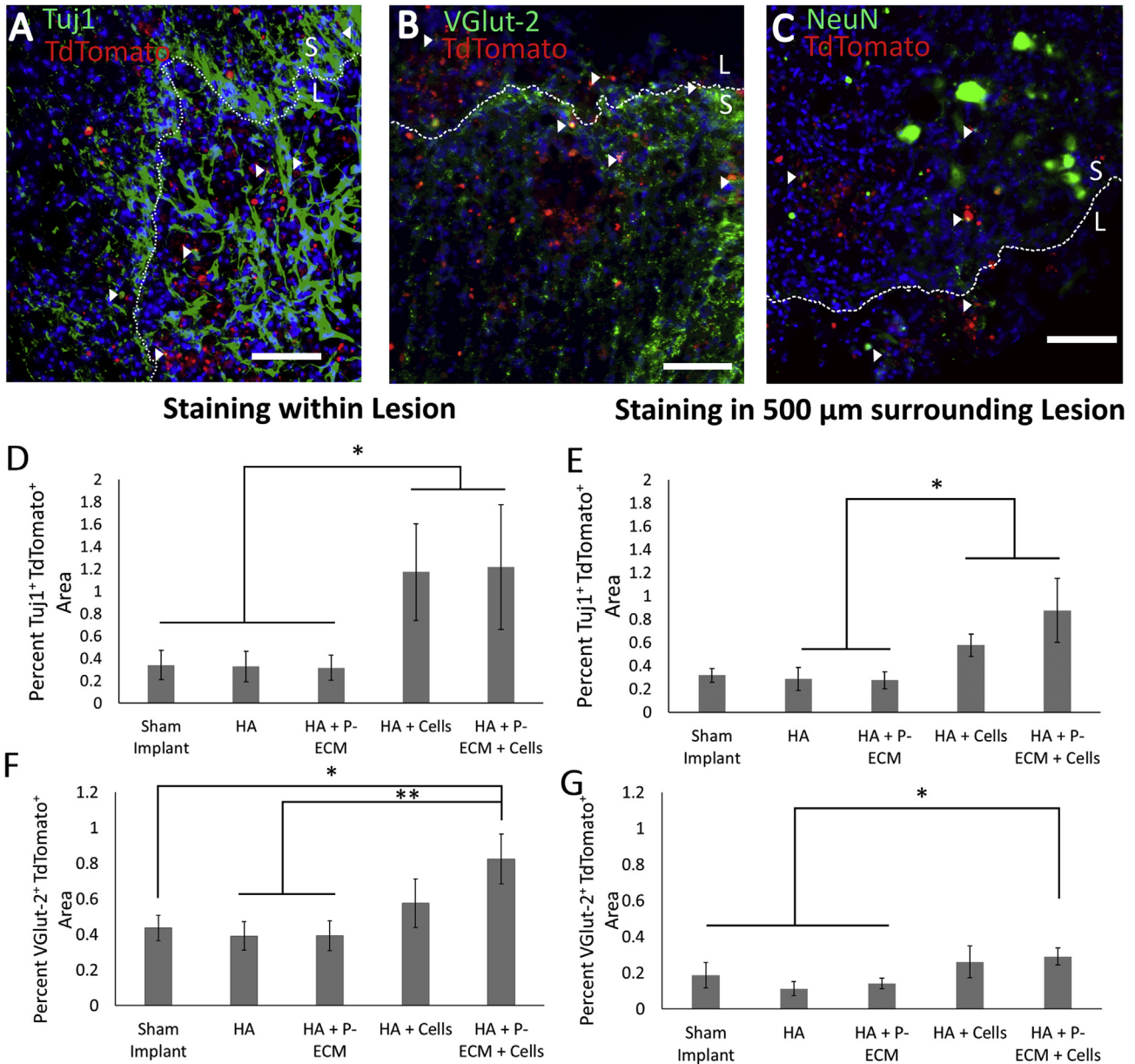


**Fig. 8. Transplanted V2a Interneurons maintain identity and enter the host spinal cord** A-C) 20× magnification of the lesion boundary in animal transplanted with HA + P-ECM + Cells showing locations where  $\beta$ -tubulin III (A), VGLUT2 (B), or NeuN (C) staining colocalizes with TdTomato (arrowheads) both within the lesion (L) and in the glial scar (S). Scale bar: 100  $\mu$ m. D-E) Percent of area within the lesion (D) and in the 500  $\mu$ m surrounding the lesion (E) staining positive for both TdTomato and  $\beta$ -tubulin III. F-G) Percent of area within the lesion (F) and in the 500  $\mu$ m surrounding the lesion (G) staining positive for both TdTomato and VGLUT-2. \*:  $p < 0.05$ , \*\*:  $p < 0.01$ .  $n = 7$  for Sham, HA, and HA + Proto ECM, 8 for HA + Cells and HA + Proto ECM + Cells.

#### 4.2. P-ECM decreases immune cell infiltration both in and around the SCI lesion

Since the ECM transplants were xenogenic, it was important to ensure that they were not being rejected by the host. Consistent with previous decellularized ECM implantation studies [23], no increase in immune cell infiltration was observed in any of the ECM implant groups despite an immunocompetent host in the acellular implant study (Fig. 3). In fact, the data indicated that P-ECM, but not F-ECM, resulted in a decrease in myeloid cell and macrophage/microglia infiltration in the 500  $\mu$ m surrounding the lesion compared to sham implantation (Fig. 3). Furthermore, HA:P-ECM implantation was found to significantly reduce myeloid cell staining within the lesion compared to all other groups (Fig. 3). This

observation suggests that P-ECM may exhibit an immunomodulatory role within the spinal cord. It is also important to note that HA hydrogels have been found to attenuate the inflammatory response, based on ED-1 staining, when injected acutely following injury [54,55]. In the present study a delayed implantation model was used and we did not observe any changes to the myeloid cell response in either the HA-furan or HA-methylfuran group compared to sham.

ECM-dependent immune modulation has been previously described in the transplantation of other ECM materials [56], and has been observed in transplantation of either decellularized urinary bladder or decellularized whole spinal cord ECM following SCI [57]. One potential explanation for P-ECM, but not F-ECM, displaying evidence of immunomodulation is the presence of

significantly more fibronectin and laminin in P-ECM. Fibronectin and laminin together have been found to cause tumor necrosis factor alpha (TNF- $\alpha$ ), a known pro-inflammatory cytokine, to bind to fibronectin and adopt a pro-adhesive function [58]. This binding of TNF- $\alpha$  limits its diffusion and could help to control and localize the inflammatory response.

Another possible explanation is that P-ECM may alter the ratio of classically activated M1 macrophages, that cause tissue destruction, to “alternatively” activated M2 macrophages, which have been shown to be important to normal tissue repair throughout the body and CNS [59]. In support of this idea, decreased macrophage infiltration and increased M2 macrophage presence has been described in response to implantation of increasing concentrations of decellularized urinary bladder ECM into a stroke cavity [60]. Based on these studies, it would be potentially enlightening to explore the macrophage activation state following P-ECM implantation to determine if P-ECM implantation is causing an increase in the presence of M2 macrophages. Overall, the immunomodulation effects observed in this study are a relatively unique advantage of ECM-based treatments, since many materials used for implantation are immunologically inert.

#### 4.3. Protoplasmic, but not fibrous, astrocyte ECM improves neuron growth on acellular HA hydrogels both *in vivo* and *in vitro*

*In vitro* motoneuron growth assays on thin HA hydrogels found that both F-ECM and P-ECM increased average neurite extension. P-ECM exhibited more potency demonstrating an effect at a 1:100 wt ratio of ECM to HA, while no significant effect was observed with F-ECM until a 1:25 wt ratio (Fig. 2). These *in vitro* findings were somewhat replicated in the *in vivo* implantation studies with 1:100 P-ECM:HA hydrogel implantation resulting in significantly more axon growth into the SCI lesion than when a 1:100 F-ECM:HA hydrogel or nothing was implanted (Fig. 5). Both ECMs were used at 1:100 ratios for the *in vivo* studies to better facilitate comparison between them. P-ECM incorporation was also found to increase axon growth in the HA-mF hydrogel system with acellular P-ECM:HA-mF hydrogels demonstrating significantly more axon growth into the lesion compared to HA-mF alone hydrogels and sham implant animals. Previous studies have shown implantation of either decellularized fetal spinal cord or urinary bladder ECM following dorsal hemisection SCI increases neuronal growth, supporting the idea that the naïve spinal cord ECM could have regenerative properties [57].

In both *in vivo* studies, there is an observable inverse correlation in the acellular treatment groups between the percent GFAP<sup>+</sup> area in the 500  $\mu$ m surrounding the lesion and the percent  $\beta$ -tubulin III<sup>+</sup> area within the lesion (Figs. 4–7). This suggests that the axonal growth benefits observed in the presence of P-ECM may be related to a phenotypic switch of the native astrocytes to a less reactive state. Further experimentation is required to determine the precise nature of any astrocyte phenotype change and what specific factors within the implanted ECMs might be responsible for these changes.

#### 4.4. V2a interneurons survive within HA hydrogels, migrate/extend processes into the host, and increase neuronal process area both within and around the SCI lesion regardless of P-ECM presence

Quantification of the continued presence of the V2a interneuron neuroaggregates, using TdTomato fluorescence, revealed that both HA-mF hydrogels and P-ECM:HA-mF supported cellular transplantation (Fig. 7). Staining for  $\beta$ -tubulin III revealed that the presence of V2a neuroaggregates led to a significant increase in neuronal processes within and around the lesion area. This V2a interneuron-associated increase in neuronal process staining could

be the result of two different sources: growth from the transplanted interneurons, and/or increased axon ingrowth from the host promoted by the interneurons within the lesion. Quantification of the colocalization TdTomato and  $\beta$ -tubulin III suggests that a combination of these two effects is occurring, since the TdTomato<sup>+</sup> neuronal processes only explain some of the observed increase in neuronal processes (Fig. 8D–E). Colocalization analysis also revealed that some TdTomato<sup>+</sup> processes entered the host spinal cord, indicating that these transplanted cells might be able to integrate with the host or at least are able to move out the lesion site itself (Fig. 8E). The ability of the transplanted cells to migrate into the host is further supported by the presence of NeuN<sup>+</sup> TdTomato<sup>+</sup> nuclei in the region surrounding the lesion (Fig. 8C). Analysis of VGlut-2 staining showed that VGlut-2<sup>+</sup> TdTomato<sup>+</sup> pixels represented a significantly larger percent of the area within and around the lesion in the HA + P-ECM + Cells group than observed in any acellular group (Fig. 8F–G). This finding indicates that the transplanted V2as are maintaining a glutamatergic identity following transplantation.

Overall, neuronal staining data demonstrated that either V2a interneuron neuroaggregate transplantation or P-ECM incorporation conferred a significant benefit on neuronal growth compared to HA alone, but the combination of these factors did not significantly increase the area staining positive for neuronal processes (Fig. 7). Importantly, TdTomato colocalization with NeuN, VGlut-2, and  $\beta$ -tubulin III indicates that the transplanted V2a interneurons maintain their identity as glutamatergic neurons, migrate into the host, and extend neuronal processes both within the lesion and into the surrounding cord (Fig. 8). Future long-term recovery studies will be required to determine if these transplanted V2a interneurons are able to functionally integrate into the host spinal cord, and if the presence V2a interneurons and/or the increased neuronal area caused by P-ECM incorporation translates into any behavioral improvements.

This work, as a whole, demonstrates that mESC-derived P-ECM, but not F-ECM, incorporation into HA hydrogels results in significant improvements in histological markers of recovery following SCI. Furthermore, ECM implantation was found to alter the behavior of immune cells, astrocytes, and neurons within the context of the injured spinal cord, showing the multifactorial functionality of the HA:P-ECM material. The HA hydrogels were also found to support the transplantation of V2a interneurons into the SCI lesion and the presence of these cells was found to cause similar increases in neuronal process staining to those observed with P-ECM implantation. HA is the primary component of the native CNS ECM and HA alone implantation was found to decrease CSPG staining around the lesion, and support cellular transplantation. These observations indicate that HA may be preferable to other materials for CNS injury treatment. This work also shows that mESCs can be used as a scalable source of bioactive ECM as well as a source of V2a interneurons. The use of mESCs increases the potential clinical impact of this work, since the materials used do not require donor tissue to be generated.

#### Competing interests

The authors have no competing interests to declare.

#### Acknowledgements

The authors gratefully acknowledge Dr. Nisha Iyer for her assistance with the V2a differentiation and aggregation protocols and the veterinary staff at the University of Texas at Austin Animal Resources Center for their assistance with the care of the subjects of this work. This work was supported by NINDS R01 NS090617, the

Washington University Medical Scientist Training Program (NIH T32 GM07200), the University of Texas at Austin and the Canadian Institutes of Health Research (CIHR Foundation grant to MSS) and the Natural Sciences and Engineering Research Council of Canada (NSERC Discovery to MSS and PGSD to LS).

## Appendix A. Supplementary data

Supplementary data related to this article can be found at <https://doi.org/10.1016/j.biomaterials.2018.02.013>.

## References

- [1] J.M. Cregg, M.A. DePaul, A.R. Filous, B.T. Lang, A. Tran, J. Silver, Functional regeneration beyond the glial scar, *Exp. Neurol.* 253 (2014) 197–207, <https://doi.org/10.1016/j.expneurol.2013.12.024>.
- [2] A. Oohira, F. Matsui, R. Katoh-Semba, Inhibitory effects of brain chondroitin sulfate proteoglycans on neurite outgrowth from PC12D cells, *J. Neurosci.* 11 (1991) 822–827. <http://www.ncbi.nlm.nih.gov/pubmed/2002362>. (Accessed 13 May 2017).
- [3] E.J. Bradbury, L.D.F. Moon, R.J. Popat, V.R. King, G.S. Bennett, P.N. Patel, J.W. Fawcett, S.B. McMahon, Chondroitinase ABC promotes functional recovery after spinal cord injury, *Nature* 416 (2002) 636–640, <https://doi.org/10.1038/416636a>.
- [4] T.S. Wilems, S.E. Sakiyama-Elbert, Sustained dual drug delivery of anti-inhibitory molecules for treatment of spinal cord injury, *J. Contr. Release* 213 (2015) 103–111, <https://doi.org/10.1016/j.jconrel.2015.06.031>.
- [5] J.R. Faulkner, J.E. Herrmann, M.J. Woo, K.E. Tansey, N.B. Doan, M. V Sofroniew, Reactive astrocytes protect tissue and preserve function after spinal cord injury, *J. Neurosci.* 24 (2004) 2143–2155, <https://doi.org/10.1523/JNEUROSCI.3547-03.2004>.
- [6] M.A. Anderson, J.E. Burda, Y. Ren, Y. Ao, T.M. O'Shea, R. Kawaguchi, G. Coppola, B.S. Khakh, T.J. Deming, M.V. Sofroniew, Astrocyte scar formation aids central nervous system axon regeneration, *Nature* 532 (2016) 195–200, <https://doi.org/10.1038/nature17623>.
- [7] S.A. Liddelow, B.A. Barres, Reactive astrocytes: production, function, and therapeutic potential, *Immunity* 46 (2017) 957–967, <https://doi.org/10.1016/j.immuni.2017.06.006>.
- [8] J.L. Zamarian, L. Xu, L.C. Foo, N. Nouri, L. Zhou, R.G. Giffard, B.A. Barres, Genomic analysis of reactive astrogliosis, *J. Neurosci.* 32 (2012) 6391–6410, <https://doi.org/10.1523/JNEUROSCI.6221-11.2012>.
- [9] E.N. Benveniste, S.M. Sparacio, J.G. Norris, H.E. Grenett, G.M. Fuller, Induction and regulation of interleukin-6 gene expression in rat astrocytes, *J. Neuroimmunol.* 30 (1990) 201–212. <http://www.ncbi.nlm.nih.gov/pubmed/2121800>. (Accessed 6 July 2017).
- [10] S. Codeluppi, T. Fernandez-Zafra, K. Sandor, J. Kjell, Q. Liu, M. Abrams, L. Olson, N.S. Gray, C.I. Svensson, P. Uhlén, Interleukin-6 secretion by astrocytes is dynamically regulated by PI3K-mTOR-calcium signaling, *PLoS One* 9 (2014), e92649, <https://doi.org/10.1371/journal.pone.0092649>.
- [11] C.A. Jackson, J. Messinger, J.D. Peduzzi, D.C. Ansardi, C.D. Morrow, Enhanced functional recovery from spinal cord injury following intrathecal or intramuscular administration of poliovirus replicons encoding IL-10, *Virology* 336 (2005) 173–183, <https://doi.org/10.1016/j.virol.2005.03.025>.
- [12] D. Sun, M. Lye-Barthel, R.H. Masland, T.C. Jakobs, Structural remodeling of fibrous astrocytes after axonal injury, *J. Neurosci.* 30 (2010) 14008–14019, <https://doi.org/10.1523/JNEUROSCI.3605-10.2010>.
- [13] U. Wilhelmsson, E.A. Bushong, D.L. Price, B.L. Smarr, V. Phung, M. Terada, M.H. Ellisman, M. Pekny, Redefining the concept of reactive astrocytes as cells that remain within their unique domains upon reaction to injury, *Proc. Natl. Acad. Sci.* 103 (2006) 17513–17518, <https://doi.org/10.1073/pnas.0602841103>.
- [14] J.E. Davies, C. Pröschel, N. Zhang, M. Noble, M. Mayer-Pröschel, S.J.A. Davies, Transplanted astrocytes derived from BMP- or CNTF-treated glial-restricted precursors have opposite effects on recovery and allodynia after spinal cord injury, *J. Biol.* 7 (2008) 24, <https://doi.org/10.1186/jbiol85>.
- [15] S.J.A. Davies, C.-H. Shih, M. Noble, M. Mayer-Pröschel, J.E. Davies, C. Pröschel, Transplantation of specific human astrocytes promotes functional recovery after spinal cord injury, *PLoS One* 6 (2011), e17328, <https://doi.org/10.1371/journal.pone.0017328>.
- [16] R.E. Thompson, A. Lake, P. Kenny, M. Saunders, K. Sakers, N. Iyer, J.D. Dougherty, S.E. Sakiyama-Elbert, Different mixed astrocyte populations derived from embryonic stem cells have variable neuronal growth support capacities, *Stem Cell. Dev.* (2017), <https://doi.org/10.1089/scd.2017.0121>.
- [17] S.F. Badyalak, D.O. Freytes, T.W. Gilbert, Extracellular matrix as a biological scaffold material: structure and function, *Acta Biomater.* 5 (2009) 1–13, <https://doi.org/10.1016/j.actbio.2008.09.013>.
- [18] K.E.M. Benders, P.R. van Weeren, S.F. Badyalak, D.B.F. Saris, W.J.A. Dhert, J. Malda, Extracellular matrix scaffolds for cartilage and bone regeneration, *Trends Biotechnol.* 31 (2013) 169–176, <https://doi.org/10.1016/j.tibtech.2012.12.004>.
- [19] A.M. Moore, M. MacEwan, K.B. Santosa, K.E. Chenard, W.Z. Ray, D.A. Hunter, S.E. Mackinnon, P.J. Johnson, Acellular nerve allografts in peripheral nerve regeneration: a comparative study, *Muscle Nerve* 44 (2011) 221–234, <https://doi.org/10.1002/mus.22033>.
- [20] J.M. Singelyn, P. Sundaramurthy, T.D. Johnson, P.J. Schup-Magoffin, D.P. Hu, D.M. Faulk, J. Wang, K.M. Mayle, K. Bartels, M. Salvatore, A.M. Kinsey, A.N. Demaria, N. Dib, K.L. Christman, Catheter-deliverable hydrogel derived from decellularized ventricular extracellular matrix increases endogenous cardiomyocytes and preserves cardiac function post-myocardial infarction, *J. Am. Coll. Cardiol.* 59 (2012) 751–763, <https://doi.org/10.1016/j.jacc.2011.10.888>.
- [21] S.B. Seif-Naraghi, J.M. Singelyn, M.A. Salvatore, K.G. Osborn, J.J. Wang, U. Sampat, O.L. Kwan, G.M. Strachan, J. Wong, P.J. Schup-Magoffin, R.L. Braden, K. Bartels, J.A. DeQuach, M. Preul, A.M. Kinsey, A.N. DeMaria, N. Dib, K.L. Christman, Safety and efficacy of an injectable extracellular matrix hydrogel for treating myocardial infarction, *Sci. Transl. Med.* 5 (2013), <https://doi.org/10.1126/scitranslmed.3005503>, 173ra25.
- [22] S.-H. Mirmalek-Sani, D.C. Sullivan, C. Zimmerman, T.D. Shupe, B.E. Petersen, Immunogenicity of decellularized porcine liver for bioengineered hepatic tissue, *Am. J. Pathol.* 183 (2013) 558–565, <https://doi.org/10.1016/j.ajpath.2013.05.002>.
- [23] T.W. Hudson, S. Zawko, C. Deister, S. Lundy, C.Y. Hu, K. Lee, C.E. Schmidt, Optimized acellular nerve graft is immunologically tolerated and supports regeneration, *Tissue Eng.* 10 (1641–51), <https://doi.org/10.1089/ten.2004.10.1641>.
- [24] K.M. Yamada, D.W. Kennedy, K. Kimata, R.M. Pratt, Characterization of fibronectin interactions with glycosaminoglycans and identification of active proteolytic fragments, *J. Biol. Chem.* 255 (1980) 6055–6063. <http://www.ncbi.nlm.nih.gov/pubmed/6771264>. (Accessed 4 November 2017).
- [25] A. Bignami, M. Hosley, D. Dahl, Hyaluronic acid and hyaluronic acid-binding proteins in brain extracellular matrix, *Anat. Embryol. (Berl)* 188 (1993) 419–433. <http://www.ncbi.nlm.nih.gov/pubmed/7508695>. (Accessed 13 September 2015).
- [26] C.M. Nimmo, S.C. Owen, M.S. Shoichet, Diels-Alder Click cross-linked hyaluronic acid hydrogels for tissue engineering, *Biomacromolecules* 12 (2011) 824–830, <https://doi.org/10.1021/bm101446k>.
- [27] T. Führmann, J. Obermeyer, C.H. Tator, M.S. Shoichet, Click-crosslinked injectable hyaluronic acid hydrogel is safe and biocompatible in the intrathecal space for ultimate use in regenerative strategies of the injured spinal cord, *Methods* 84 (2015) 60–69, <https://doi.org/10.1016/j.jymeth.2015.03.023>.
- [28] M.A. Matthews, M.F. St Onge, C.L. Faciane, J.B. Gelderd, Spinal cord transection: a quantitative analysis of elements of the connective tissue matrix formed within the site of lesion following administration of piromen, cytoxin or trypsin., *Neuropathol. Appl. Neurobiol.* 5 (n.d.) 161–180. <http://www.ncbi.nlm.nih.gov/pubmed/471188> (accessed November 15, 2016).
- [29] G. Courtine, B. Song, R.R. Roy, H. Zhong, J.E. Herrmann, Y. Ao, J. Qi, V.R. Edgerton, M. V Sofroniew, Recovery of supraspinal control of stepping via indirect propriospinal relay connections after spinal cord injury, *Nat. Med.* 14 (2008) 69–74, <https://doi.org/10.1038/nm1682>.
- [30] S.A. Crone, K.A. Quinlan, L. Zagoraoui, S. Droho, C.E. Restrepo, L. Lundfeld, T. Endo, J. Setlak, T.M. Jessell, O. Kiehn, K. Sharma, Genetic ablation of V2a ipsilateral interneurons disrupts left-right locomotor coordination in mammalian spinal cord, *Neuron* 60 (2008) 70–83, <https://doi.org/10.1016/j.neuron.2008.08.009>.
- [31] S.A. Crone, G. Zhong, R. Harris-Warrick, K. Sharma, In mice lacking V2a interneurons, gait depends on speed of locomotion, *J. Neurosci.* 29 (2009) 7098–7109, <https://doi.org/10.1523/JNEUROSCI.1206-09.2009>.
- [32] L.V. Zholdudeva, J.S. Karliner, K.J. Dougherty, M.A. Lane, Anatomical recruitment of spinal V2a interneurons into phrenic motor circuitry after high cervical spinal cord injury, *J. Neurotrauma* (2017), <https://doi.org/10.1089/neu.2017.5045>.
- [33] N.R. Iyer, J.E. Huettner, J.C. Butts, C.R. Brown, S.E. Sakiyama-Elbert, Generation of highly enriched V2a interneurons from mouse embryonic stem cells, *Exp. Neurol.* 277 (2016) 305–316, <https://doi.org/10.1016/j.expneurol.2016.01.011>.
- [34] C.R. Brown, J.C. Butts, D.A. McCreedy, S.E. Sakiyama-Elbert, Generation of v2a interneurons from mouse embryonic stem cells, *Stem Cell. Dev.* 23 (2014) 1765–1776, <https://doi.org/10.1089/scd.2013.0628>.
- [35] L. Roybon, N. Lamas, A. Garcia-Diaz, E. Yang, R. Sattler, V. Jackson-Lewis, Y. Kim, C.A. Kachel, J. Rothstein, S. Przedborski, H. Wichterle, C. Henderson, Human stem cell-derived spinal cord astrocytes with defined mature or reactive phenotypes, *Cell Rep.* 4 (2013) 1035–1048, <https://doi.org/10.1016/j.celrep.2013.06.021>.
- [36] T.W. Hudson, S.Y. Liu, C.E. Schmidt, Engineering an improved acellular nerve graft via optimized chemical processing, *Tissue Eng.* 10 (2004) 1346–1358, <https://doi.org/10.1089/ten.2004.10.1346>.
- [37] S. McDevitt, Todd C Butts, Jessica C. Iyer, Nisha; White, Nick; Thompson, Russell E; Sakiyama-Elbert, V2a Interneuron Differentiation from Mouse and Human Pluripotent Stem Cells, *Prep.* (n.d.).
- [38] D.A. McCreedy, T.S. Wilems, H. Xu, J.C. Butts, C.R. Brown, A.W. Smith, S.E. Sakiyama-Elbert, Survival, differentiation, and migration of high-purity mouse embryonic stem cell-derived progenitor motor neurons in fibrin scaffolds after sub-acute spinal cord injury, *Biomater. Sci.* 2 (2014) 1672–1682, <https://doi.org/10.1039/c4bm00106k>.
- [39] S.J. Taylor, S.E. Sakiyama-Elbert, Effect of controlled delivery of neurotrophin-3 from fibrin on spinal cord injury in a long term model, *J. Contr. Release* 116

- (2006) 204–210, <https://doi.org/10.1016/j.jconrel.2006.07.005>.
- [40] L.J. Smith, S.M. Taimoory, R.Y. Tam, A.E.G. Baker, N.B. Mohammad, J.F. Trant, M. Shoichet, Diels-alder click-crosslinked hydrogels with increased reactivity enable 3D cell encapsulation, *Biomacromolecules*. (n.d.).
- [41] A. Etlin, J.M. Bráz, J.A. Kuhn, X. Wang, K.A. Hamel, I.J. Llewellyn-Smith, A.I. Basbaum, Functional synaptic integration of forebrain GABAergic precursors into the adult spinal cord, *J. Neurosci.* 36 (2016) 11634–11645, <https://doi.org/10.1523/JNEUROSCI.2301-16.2016>.
- [42] T.M. Fandel, A. Trivedi, C.R. Nicholas, H. Zhang, J. Chen, A.F. Martinez, L.J. Noble-Haesslein, A.R. Kriegstein, Transplanted human stem cell-derived interneuron precursors mitigate mouse bladder dysfunction and central neuropathic pain after spinal cord injury, *Cell Stem Cell.* 19 (2016) 544–557, <https://doi.org/10.1016/j.stem.2016.08.020>.
- [43] Z.Z. Khaing, B.D. Milman, J.E. Vanscoy, S.K. Seidlits, R.J. Grill, C.E. Schmidt, High molecular weight hyaluronic acid limits astrocyte activation and scar formation after spinal cord injury, *J. Neural. Eng.* 8 (2011), 46033, <https://doi.org/10.1088/1741-2560/8/4/046033>.
- [44] Y. Wen, S. Yu, Y. Wu, R. Ju, H. Wang, Y. Liu, Y. Wang, Q. Xu, Spinal cord injury repair by implantation of structured hyaluronic acid scaffold with PLGA microspheres in the rat, *Cell Tissue Res.* 364 (2016) 17–28, <https://doi.org/10.1007/s00441-015-2298-1>.
- [45] M.S. Pandey, B.A. Baggenstoss, J. Washburn, E.N. Harris, P.H. Weigel, The hyaluronan receptor for endocytosis (HARE) activates NF- $\kappa$ B-mediated gene expression in response to 40–400-kDa, but not smaller or larger, hyaluronans, *J. Biol. Chem.* 288 (2013) 14068–14079, <https://doi.org/10.1074/jbc.M112.442889>.
- [46] M.L. Lemons, D.R. Howland, D.K. Anderson, Chondroitin sulfate proteoglycan immunoreactivity increases following spinal cord injury and transplantation, *Exp. Neurol.* 160 (1999) 51–65, <https://doi.org/10.1006/exnr.1999.7184>.
- [47] M.M. Pakulska, C.H. Tator, M.S. Shoichet, Local delivery of chondroitinase ABC with or without stromal cell-derived factor 1 $\alpha$  promotes functional repair in the injured rat spinal cord, *Biomaterials* 134 (2017) 13–21, <https://doi.org/10.1016/j.biomaterials.2017.04.016>.
- [48] P.J. Johnson, S.R. Parker, S.E. Sakiyama-Elbert, Controlled release of neurotrophin-3 from fibrin-based tissue engineering scaffolds enhances neural fiber sprouting following subacute spinal cord injury, *Biotechnol. Bioeng.* 104 (2009) 1207–1214, <https://doi.org/10.1002/bit.22476>.
- [49] P.J. Johnson, A. Tatar, D.A. McCreedy, A. Shiu, S.E. Sakiyama-Elbert, Tissue-engineered fibrin scaffolds containing neural progenitors enhance functional recovery in a subacute model of SCI, *Soft Matter* 6 (2010) 5127–5137, <https://doi.org/10.1039/c0sm00173b>.
- [50] B. Du, C. Zeng, W. Zhang, D. Quan, E. Ling, Y. Zeng, A comparative study of gelatin sponge scaffolds and PLGA scaffolds transplanted to completely transected spinal cord of rat, *J. Biomed. Mater. Res. Part A* 102 (2014) 1715–1725, <https://doi.org/10.1002/jbm.a.34835>.
- [51] M. Hara, K. Kobayakawa, Y. Ohkawa, H. Kumamaru, K. Yokota, T. Saito, K. Kijima, S. Yoshizaki, K. Harimaya, Y. Nakashima, S. Okada, Interaction of reactive astrocytes with type I collagen induces astrocytic scar formation through the integrin–N-cadherin pathway after spinal cord injury, *Nat. Med.* 23 (2017) 818–828, <https://doi.org/10.1038/nm.4354>.
- [52] V.M. Tysseling-Mattiace, V. Sahni, K.L. Niece, D. Birch, C. Czeisler, M.G. Fehlings, S.I. Stupp, J.A. Kessler, Self-assembling nanofibers inhibit glial scar formation and promote axon elongation after spinal cord injury, *J. Neurosci.* 28 (2008) 3814–3823, <https://doi.org/10.1523/JNEUROSCI.0143-08.2008>.
- [53] T.W. Hsiao, P.A. Tresco, V. Hlady, Astrocytes alignment and reactivity on collagen hydrogels patterned with ECM proteins, *Biomaterials* 39 (2015) 124–130, <https://doi.org/10.1016/j.biomaterials.2014.10.062>.
- [54] D. Gupta, C.H. Tator, M.S. Shoichet, Fast-gelling injectable blend of hyaluronan and methylcellulose for intrathecal, localized delivery to the injured spinal cord, *Biomaterials* 27 (2006) 2370–2379, <https://doi.org/10.1016/j.biomaterials.2005.11.015>.
- [55] J.W. Austin, C.E. Kang, M.D. Baumann, L. DiDiodato, K. Satkunendrarajah, J.R. Wilson, G.J. Stanisz, M.S. Shoichet, M.G. Fehlings, The effects of intrathecal injection of a hyaluronan-based hydrogel on inflammation, scarring and neurobehavioural outcomes in a rat model of severe spinal cord injury associated with arachnoiditis, *Biomaterials* 33 (2012) 4555–4564, <https://doi.org/10.1016/j.biomaterials.2012.03.022>.
- [56] J.L. Dziki, L. Huleihel, M.E. Scarritt, S.F. Badylak, Extracellular matrix Bioscaffolds as immunomodulatory biomaterials, *Tissue Eng. Part A* (2017), <https://doi.org/10.1089/ten.tea.2016.0538>.
- [57] D. Tukmachev, S. Forostyak, Z. Koci, K. Zaviskova, I. Vackova, K. Vyborny, I. Sandvig, A. Sandvig, C.J. Medberry, S.F. Badylak, E. Sykova, S. Kubinova, Injectable extracellular matrix hydrogels as scaffolds for spinal cord injury repair, *Tissue Eng. Part A* 22 (2016) 306–317, <https://doi.org/10.1089/ten.TEA.2015.0422>.
- [58] R. Hershkovich, I. Goldkorn, O. Lider, Tumour necrosis factor-alpha interacts with laminin and functions as a pro-adhesive cytokine, *Immunology* 85 (1995) 125–130, <http://www.ncbi.nlm.nih.gov/pubmed/7635514>. (Accessed 21 August 2017).
- [59] K.A. Kigerl, J.C. Gensel, D.P. Ankeny, J.K. Alexander, D.J. Donnelly, P.G. Popovich, Identification of two distinct macrophage subsets with divergent effects causing either neurotoxicity or regeneration in the injured mouse spinal cord, *J. Neurosci.* 29 (2009) 13435–13444, <https://doi.org/10.1523/JNEUROSCI.3257-09.2009>.
- [60] H. Ghuman, A.R. Massensini, J. Donnelly, S.-M. Kim, C.J. Medberry, S.F. Badylak, M. Modo, ECM hydrogel for the treatment of stroke: characterization of the host cell infiltrate, *Biomaterials* 91 (2016) 166–181, <https://doi.org/10.1016/j.biomaterials.2016.03.014>.
- [61] L.J. Smith, S.M. Taimoory, R.Y. Tam, A.E.G. Baker, N.B. Mohammad, J.F. Trant, M.S. Shoichet, Diels-alder click-crosslinked hydrogels with increased reactivity enable 3D cell encapsulation, *Biomacromolecules* (2018) (in press).